Investigating the Near-Infrared Properties of Planetary Nebulae II. Medium Resolution Spectra

Joseph L. Hora
Smithsonian Astrophysical Observatory, 60 Garden Street MS/65, Cambridge, MA 02138

William B. Latter
SIRTF Science Center/Infrared Processing and Analysis Center, MS 100-22, Caltech, Pasadena, CA 91125

Lynne K. Deutsch
Astronomy Department, Boston University, 725 Commonwealth Avenue, Boston, MA 02215

ABSTRACT

We present medium-resolution (R~700) near-infrared ($\lambda = 1 - 2.5$ μm) spectra of a sample of planetary nebulae (PNe). A narrow slit was used which sampled discrete locations within the nebulae; observations were obtained at one or more positions in the 41 objects included in the survey. The PN spectra fall into one of four general categories: H I emission line-dominated PNe, H I and H_2 emission line PNe, H_2 emission line-dominated PNe, and continuum-dominated PNe. These categories correlate with morphological type, with the elliptical PNe falling into the first group, and the bipolar PNe primarily in the H_2 and continuum emission groups. The catagories also correlate with C/O ratio, with the O-rich objects falling into the first group and the C-rich objects in the groups. Other spectral features were observed in all catagories, such as continuum emission from the central star, and warm dust continuum emission towards the long wavelength end of the spectra.

H_2 was detected in four PNe in this survey for the first time. An analysis was performed using the H_2 line ratios in all of the PN spectra in the survey where a sufficient number of lines were observed to determine the ortho-to-para ratio and the rotational and vibrational excitation temperatures of the H_2 in those objects. One unexpected result from this analysis is that the H_2 is excited by absorption of ultraviolet photons in most of the PNe, although there are several PNe in which collisional excitation plays an important role. The correlation between bipolar morphology and H_2 emission has been strengthened with the new detections of H_2 in this survey.

Subject headings: planetary nebulae: general - ISM: molecules - ISM: structure - infrared: ISM: continuum - infrared: ISM: lines and bands - molecular processes

1. Introduction

This is the second of two papers describing the results of surveys of the properties of planetary nebulae (PNe) in the near-infrared ($\lambda = 1 - 2.5$ μm). The first paper (Latter et al. 1995; hereafter Paper I) presented an infrared imaging survey; here we present the results of a near-infrared spectral survey.

There are several reasons why knowledge of the near-infrared (near-IR) characteristics of PNe is important, as described in Paper I. In order to interpret the imaging results, we must examine the spectra of these objects to understand the processes responsible for the emission. There are many emission lines present in the 1 - 2.5 μm spectral region, most notably those due to recombination lines of H I, and lines from vibrationally excited H_2. Also present are atomic lines of He I and [Fe II], and emission from other molecular species such as CO and C_2. These lines can act as diagnostic tools to probe the physical conditions inside the nebula, sampling different regions and ranges of temperature, density, and excitation than is seen by observing the optical line emission. Some PNe also exhibit strong continuum emission in the near-IR from hot dust. This emission becomes significant longward of $\lambda = 2$ μm in many of the PNe, requiring near-IR spectroscopy to detect it and to differentiate between line and continuum emission sources. Finally, the lower optical depth of the PNe in the IR as compared to optical wavelengths allows us to potentially see into regions of the nebula that are obscured by dust.

There have been several previous surveys that have explored the properties of PNe in the infrared. Early spectroscopic and photometric surveys (e.g., Gillett, Merrill, & Stein 1972, Cohen & Barlow 1974) determined that there was an excess of IR emission over what was expected from reflected continuum emission from the central star. Other photometric surveys in the following years (Whitelock 1985; Persi et al. 1987) determined the primary sources of IR emission to be stellar continuum, thermal dust emission, and thermal & line emission from the nebula itself. The near-IR color characteristics of most PNe are unique and can be used to identify new PNe and post-AGB objects (Garcia-Lario et al. 1990).

More recently there have been more detailed spectral observations of PNe in the near- IR. Hrivnak, Kwok, & Geballe (1994) surveyed a set of proto-PNe in the H and K bands. In these objects the H I Brackett lines were observed in absorption, and most objects had CO absorption or emission, indicating recent mass loss events. Rudy et al. (1992, and references therein) and Kelly & Latter (1995) have surveyed several PNe and proto-PNe in the $\lambda = 0.5 - 1.3$ μm range. Dinerstein & Crawford (1998) have completed a survey of a set of PNe in the K-band, focusing on excitation of molecular hydrogen.

There are several unique aspects of the survey results we present here that was made possible by the KSPEC spectrograph (see the instrument description below). First, because of KSPEC's high sensitivity and simultaneous sampling of the full spectral range, we were able to obtain data on a comparatively large number of objects (41) in a short period of time. Using the spectrograph's relatively narrow and short slit, we sampled different regions of the PNe to examine the emission throughout the nebula. In most of the other surveys described above, larger beams were used which included much or all of the object. Another aspect of the data presented here is that due to the cross-dispersed design of the instrument, the entire $\lambda = 1.1 - 2.5$ μm range is obtained at once, eliminating the possibility of telescope pointing errors or other fluctuations affecting the relative line strengths in the spectra. Finally, the slit-viewing detector allowed precise positioning and guiding, so the region of the PN being observed was well known for each spectrum. The PNe observed in this survey were chosen to overlap with the near-IR imaging survey (Paper I), along with several other optically-bright PNe and unresolved objects that were not included in the imaging survey.

2. Observations and Data Reduction

The observations were performed on several runs during the period 1992 October through 1994 September at the University of Hawaii 2.2m telescope on Mauna Kea, using the near-IR KSPEC spectrograph (Hodapp et al. 1994). KSPEC is a $\lambda = 1 - 2.5$ μm cross-dispersed spectrograph that has a separate slit-viewing IR array for acquiring the source and guiding. The full spectral range is obtained in a single exposure, resulting in accurate relative line measurements and highly efficient data acquisition. The diffraction orders are well- matched to the atmospheric transmission windows, with the K band in 3rd order (1.9 - 2.5 μm), H in 4th order (1.45 - 1.8 μm) and J in 5th order (1.15 - 1.32 μm). The 1×6 arcsecond slit

3.1. H I - line dominated

The line emission in these PNe is dominated by lines of H I and He I. In the J-band, the Paschen β (Paβ) line is the most intense, with contributions from lines of He I, [Fe II], and O I. In the H band, the Brackett series of H I dominate, with emission from the 1.7002 μm line of He I and 1.6440 μm line of [Fe II] present in some PNe. In the K band, the brightest line is usually Brackett γ (Brγ), with strong lines of He I at 2.058 and 2.112 μm. When the H I lines are strong enough, one begins to see the Pfund series lines starting near 2.35 μm where they are just beginning to be separated at this resolution. There are also two unidentified infrared (UIR) lines at 2.199 and 2.287 μm (Geballe et al. 1991) that appear in several PNe in this category. (Note that these UIR lines are different from the broad near- and mid-IR UIR lines usually attributed to PAHs). A few of the spectra shown here have contributions from central star continuum flux that is larger towards shorter wavelengths, or warm dust continuum that gets stronger at longer wavelengths.

3.1.1. NGC 1535

NGC 1535 is classified as early round, and its near-IR spectrum is dominated by emission lines of H I. It has a bright ionized shell of emission which is surrounded by a fainter halo (e.g., see Schwarz, Corradi, & Melnick 1992). Near-IR images were presented in Paper I. This PN has previously been observed to have H_2 lines in absorption in the far-UV (Bowers et al. 1995). Recent observations by Luhman et al. (1997) failed to detect H_2 in emission in the $v = 1 \rightarrow 0$ S(1) line. They attribute the detection in absorption at shorter wavelength to the interstellar medium, or a region in the PN itself of a much smaller size than the ionized zone.

The spectrum of NGC 1535 shown in Figure 1 was obtained at a position centered on the brightest part of the ring directly W of the central star. We also fail to detect the H_2 emission in the $v = 1 \rightarrow 0$ S(1) line, at a 1 σ level of about 5×10^{-17} ergs cm^{-2} s^{-1} Å^{-1}. There is some indication of emission from the $v = 1 \rightarrow 0$ Q(1) and $v = 1 \rightarrow 0$ Q(3) lines at the long wavelength end of the spectrum. However, the spectrum is noisier in this region and the lines are not detected above the 3 σ level.

3.1.2. NGC 2022

NGC 2022 is an early elliptical PN, but is morphologically very similar to NGC 1535 in optical images (e.g., Schwarz et al. 1992). The main difference is a different relative outer halo size as compared to the inner ring (the halo is relatively smaller in NGC 2022). Zhang & Kwok (1998) also find similar parameters in their morphological fits of these two PNe. Near-IR images of this PN were presented in Paper I.

NGC 2022 is also spectrally similar to NGC 1535, as seen in Figure 1. The spectrum of NGC 2022 was taken centered on the ring directly E of the central star. The dominant lines are those of neutral hydrogen.

3.1.3. NGC 2392

The PN NGC 2392 (the "Eskimo nebula") is another double-shell nebula; however, this PN has a significant amount of structure in the inner ring and outer shell. Spectrophotometric (Barker 1991) and kinematical studies (Reay, Atherton, & Taylor 1983; O'Dell, Weiner, & Chu 1990) that have been carried out with optical imaging and spectroscopy have revealed the abundances and ionization states and the velocities of the various components. Near-IR images of this PN were presented in Paper I.

The spectrum of NGC 2392 in Figure 1 was taken centered on the brightest part of the ring directly E of the central star. This third early-type round PN differs from the other two in Figure 1 primarily from the bright He I line at 2.058 μm, and the [Fe II] lines in the J and H bands of the spectrum.

3.1.4. NGC 3242

NGC 3242 is an early elliptical with several interesting morphological features. In addition to the bright elliptical ring, there are several filaments and knots of emission in the central region, and two ansae that are placed roughly along the major axis of the elliptical emission. Also, there is a larger faint halo that envelopes the inner structure.

Spectra acquired at three different positions on the nebula are shown in Figure 2, on the SE knot (NGC 3242SE), on the E section of the bright ring (NGC 3242E), and on the SW halo (NGC 3242H). The spectra are similar in all locations; the bright H I lines are present in all positions, along with stellar continuum at the shorter wavelengths. One difference is that the

bright ring directly SW of the central star. The SW Halo position was taken in the halo midway between the bright ring and the outer edge of the PN. The lobe and halo emission is similar, except for relatively brighter lines of He I at 1.7002 μm in the lobe. There is also some continuum emission at the short wavelength end of the nebular positions, which is probably scattered light from the central star.

3.1.11. NGC 7009

NGC 7009 (the "Saturn" nebula) is an elliptical with an interesting twisted symmetry in its shell and in the various filaments and knots of emission. Balick et al. (1998) recently published HST images that show the "microstructures" in this PN. The images show that the inner knots are actually groups of FLIERs, and jets in [N II] are seen that terminate at the tips of the nebula.

Two positions were sampled, one in the E halo region on the edge of the PN, and one in the N part of the nebula. Both positions show a contribution from stellar continuum emission from the central star. The halo emission is similar to the spectrum taken on the north edge of the PN.

3.1.12. IC 351

This compact PN has a double-lobed structure with a round halo (Hua & Grundseth 1986; Aaquist & Kwok 1990; Manchado et al. 1996). Feibelman, Hyung, & Aller (1996) obtained UV and optical spectra of IC 351 that show it to be a high excitation nebula, but without the presence of the usual silicon lines, and suggest that the silicon atoms could be locked up in grains.

This spectrum suffers from an incomplete subtraction of OH lines, due to the sky frames not being taken properly for the on-source images. The OH lines show up in emission mainly in the H and K-band portions of the spectrum. However, the major features of H I and He I emission lines can be seen.

3.1.13. IC 418

The spectrum of this well-studied young, low-excitation PN was previously shown to be dominated in the near-IR by lines of H I and He I, with a hot dust continuum (Willner et al. 1979; Zhang & Kwok 1992; Hodapp et al. 1994). Hora et al. (1993) and Paper I showed broad- and narrow-band near-IR images of the PN, showing the elliptical, double-lobed structure in the IR.

Three positions in the nebula were observed to determine the spectral variations across the object. The positions observed were on the central star, the peak of the E lobe, and in the halo region outside of the bright ring (Figure 9). In the central position, stellar continuum is visible, rising towards shorter wavelengths. The nebular lines are similar in the central and lobe positions. The halo emission is almost devoid of lines; there is some faint Paβ present as well as Brγ, this is possibly reflected from the bright lobes. The main component of the halo emission is a weak continuum that rises towards longer wavelengths.

3.1.14. IC 2149

This peculiar PN has a bright core and a roughly bipolar nebula extending roughly E-W, but does not show the usual H_2 signature of bipolar PN. The two spectra shown in Figure 10 were taken centered on the bright core, and on the E lobe. The core spectrum shows strong stellar continuum, with the nebular lines superimposed. The E lobe emission is primarily from H I and He I lines, in addition to weak continuum emission which is probably reflected from the central star.

3.1.15. IC 3568

This round PN consists of spherical shells, an inner bright one and a outer halo. Balick et al. (1987) showed that the structure was consistent with simple hydrodynamic models of PN that are shaped by interior stellar winds. The spectrum taken on the N edge of the round PN IC 3568 is shown in Figure 11. The predominant features are H I and He I emission lines, and low level continuum emission which is probably reflected from the central star.

3.1.16. IC 4593

Bohigas & Olguin (1996) obtained spectroscopy and imaging of this PN which has two inner shells surrounded by an outer highly excited halo. IC 4593 is unusual in that the condensations outside of the inner region are located asymmetrically in the SW region.

Two spectra were taken on this PN, one positioned on the central star, and the other at a position 3″ E (Figure 11). The core shows bright stellar continuum, with nebular lines superimposed, and Paβ absorption.

certain, especially if only v = 1 lines are detected. We did not attempt to determine the O/P ratio for objects without sufficient line detections. A lower than thermal O/P ratio indicates that the H_2 emission is not thermally excited. A subthermal O/P ratio is not caused by the UV excitation process itself, but is a function of chemistry and density in the PDR (e.g., Hora & Latter 1996; Black & van Dishoeck 1987). We show selected excitation diagrams for several objects that are discussed below (Figure 32).

3.2.2. NGC 40

This is the first reported detection of H_2 in NGC 40. The spectrum was taken centered on the W lobe, and the H_2 lines are relatively weak compared to the H I and He I lines from the ionized gas in this region. The H_2 emission was not detected in the narrowband imaging surveys of Paper I or Kastner et al. (1996), so the molecular emission must be confined to a region near the bright ionized gas that dominates the spectrum.

The morphological classification of NGC 40 is middle elliptical (Balick 1987), so this goes against the previously observed strong correlation between bipolar morphology and H_2 detection. However, if one examines the low-level emission in the N and S regions of this PN (see Paper I), one can see material that has broken through and expanded beyond the elliptical shell defined by the E and W bright lobes. Mellema (1995) has found the morphology consistent with models of "barrel"-shaped PNe, which have roughly cylindrical emission regions slightly bowed outwards at the equatorial plane, and less dense polar regions. Higher resolution and more sensitive optical imaging has recently been carried out by Meaburn et al. (1996) show gas escaping from the polar regions of the PN, with other filamentary structure in the outer halo. The data suggest that the H_2 is shock excited. But, insufficient line detections make this result less than firm.

3.2.3. NGC 2440

NGC 2440 is a bipolar PN with complex morphological and spectral structure. In the optical, the nebula is bipolar with the major axis in roughly the E-W direction for the large outer lobes (Balick 1987; Schwartz 1992). However, there are two bright lobes near the core that are positioned along an axis roughly perpendicular to the major axis of the outer lobes. There are two fainter knots that are also along a roughly E-W axis, but not aligned with the outer lobes. There are filaments and knots throughout the lobes. Lopez et al. (1998) finds up to three outflowing bipolar structures in the lobes, and find from their kinematic study that the inner bright lobes (their lobes "A" and "B") are the emission maxima from a radially-expanding toroid viewed nearly in the plane of the sky.

In the near-IR, the inner pairs of lobes are also prominent, but the large E-W lobes are not visible (see Paper I). Instead, there is a circular outer halo visible in H_2 that is not quite centered on the inner lobe structure. Also visible are faint H_2 "spikes" that extend from the center to the circular outer halo, roughly in the equatorial plane of the large optical E-W lobes (Latter & Hora 1998).

The spectra shown in Figure 15 were taken at two different positions in the PN: on the N lobe, and on the fainter E small knot. The N lobe exhibits H I and He I lines from the ionized gas in this region, but also has significant H_2 emission. There is also strong [Fe II] emission at 1.64 and 1.257 μm. In contrast, the E knot is predominantly H_2 emission, with the only H I lines detected being Paβ and Brγ. There is strong [Fe II] emission at 1.64 and 1.257 μm in this region as well. We did an excitation analysis for the three positions observed. UV excitation dominates, except for the NE position, for which there is insufficient data. The low value of the O/P ratio is suggestive of the H_2 emission arrising from a PDR at this location as well.

Since the inner region of NGC 2440 is morphologically complex and any line of sight through the PN is likely to intersect several distinct regions, it is probably the case that the ionized and molecular zones are not mixed as the spectra might seem to indicate, but that the slit simply includes several nebular components, or is looking through a PDR and is sampling both the molecular and the recently ionized gas.

3.2.4. NGC 6720

NGC 6720 (the "Ring Nebula") is probably the best-known PN, and is the archetype for the ring or elliptical morphology that characterizes the brightest part of the nebula. The emission is not consistent with a uniform prolate shell, however, since the ratio of flux between the edge and center of the ring is higher than expected from a limb-brightened shell

results from this survey and our imaging survey were presented in a previous paper (Hora & Latter 1996); the spectra are reproduced here for comparison with the rest of the survey.

Dinerstein et al. had mapped the inner structure and found it to be elliptical surrounding the central star; our deep H_2 images showed the emission to be tracing the edges of a cylindrical shell around the star, with faint bipolar lobes extending N-S. We also detected [Fe II] at 1.64 μm in a position along the edge of the shell, indicating a transition between the inner region around the central star and the outer nebula. The line ratios observed were in excellent agreement with predictions by theoretical H_2 fluorescence calculations, and we found no significant differences between the excitation in the two positions of the nebula that were sampled (see also Luhman & Rieke 1996).

3.2.9. IC 2003

IC 2003 is a round, high-excitation PN that has a ring of emission, with a bright knot on the S edge (Manchado et al. 1996; Zhang & Kwok 1998). Feibelman (1997) obtained IUE spectra of this PN that shows a wealth of nebular and stellar lines. The IR spectra presented in Figure 21 shows that there is little continuum from the nebula; the emission is primarily from H I lines in the J, H, and K bands. There is strong UIR emission at 2.29 μm but none detected at 2.19 μm. H_2 emission is tentatively detected in the K-band in the $v = 1 \rightarrow 0$ S(1), $v = 3 \rightarrow 2$ S(1), and $v = 1 \rightarrow 0$ Q(1) lines. Each of the lines are detected at roughly a 2σ level. The line fluxes are not reliable or numerous enough to allow fitting of the line ratios.

3.2.10. IRAS 21282+5050

The young, carbon-rich PN IRAS 21282+5050 (I21282 hereafter) has been identified as having an O7(f)-[WC11] nucleus (Cohen & Jones 1987) with possibly a binary at its center. Strong ^{12}CO has been detected in a clumpy expanding shell (Likkel et al. 1988) with elongated emission N-S. Shibata et al. (1989) believe the elongated emission suggests the presence of a dust torus in the E-W direction; however, Meixner et al. (1993) see evidence for a clumpy, expanding elliptical envelope. The elongated structure is also seen in the visible (Kwok et al. 1993). Weak continuum flux at 2 and 6 cm suggests a young PN just beginning to be ionized (Likkel et al. 1994; Meixner et al. 1993). Kwok et al. (1993) believe there has been a recent sharp drop in luminosity based on the measured CO/FIR ratio. Weak HCO^+ and ^{13}CO are present (Likkel et al. 1988).

Two positions were sampled on I21282, centered on the bright core, and offset approximately 3″ N and 3″ W. The core is dominated by continuum emission from the central star. Also present are both emission lines from the ionized gas, and H_2 features in the K-band. I21282 is compact, about 4″ in diameter at K (Paper I). The slit therefore samples a slice through the entire nebula, and as a result this spectrum does not necessarily imply that the molecular and ionized gas is mixed. The Lobe spectrum shows primarily lines of H_2 (with the OH night sky lines showing up in absorption because of imperfect sky subtraction in this spectrum). The lack of emission lines due to H I and He I in the Lobe spectrum indicates that the H_2 emission is predominantly in the outer regions of the PN. The data are suggestive of shock excitation, but this should be considered tentative.

3.2.11. M 1-16

M 1-16 is a PN with a near-IR bright central region and bipolar lobes with fast winds extending at least 35″ from the core (Schwartz et al. 1992; Aspin et al. 1993; Sahai et al. 1994). Several spectra were obtained in this PN scanning across the central region; the two positions shown in Figure 22 are on the core position and 1″ S of the core. Both positions show H_2 emission; the S position is slightly brighter in both H_2 and the ionized nebular lines. Our data reveal that the H_2 is UV excited in both regions observed. This had be suggested earlier by Aspin et al. (1993). The core shows a slight rise towards long wavelengths indicating emission from warm dust continuum.

3.2.12. M 1-92

M 1-92 ("Minkowski's Footprint") is a biplor protoplanetary nebula similar in near-IR appearance to AFGL 618, and has evidence of highly collimated outflows along the bipolar axis (Paper I; Trammell & Goodrich 1996 and reference therein). Two positions were sampled in M 1-92, one in the core and one on the NW bipolar lobe. There are problems with the sky background subtraction in both spectra, which are most prominent in the $\lambda = 1.9 - 2.1$ μm region of the spectrum, but also contribute to a lower signal to noise ratio (S/N) over the whole dataset. Nevertheless, the primary characteristics are apparent. The

central star temperatures differ by about a factor of 5. The visible spectrum shows many emission lines characteristic of ionized gas (Westbrook et al. 1975), with a small H II region surrounding the central object (Carsenty & Solf 1982). The near-IR spectrum of AFGL 618 is also dominated by rotation-vibration lines of H_2 (Thronson 1981; Thronson 1983; Latter et al. 1992; Paper I).

AFGL 618 exhibits a rich spectrum of molecular line emission (Lo and Bechis 1976; Knapp et al. 1982; Cernicharo et al. 1989; Kahane et al. 1992; Martin-Pintado & Bachiller 1992; Bachiller et al. 1997; Young 1997). The lines detected include ^{12}CO, ^{13}CO, $C^{17}O$, $C^{18}O$, CS, NH_3, HCN, HCO^+, CN, and C I.

Two of the positions sampled are presented here in Figure 27 – the core spectrum and one taken 2.″4 E of the core. Both spectra show strong H_2 emission, along with [Fe II] and weak Paβ and Brγ. In addition, the core has a warm dust continuum that is apparent throughout the spectrum, and clear CO bandhead features in the 2.3 – 2.4 μm region. The CO features are also present but at lower levels in the 2.″4 E spectrum position. Our analysis of the H_2 spectrum confirms the earlier results by Latter et al. (1992) – the spectrum is dominated by a shock heated component, but a UV excited component is clearly present as well (Figure 32c).

3.3.4. AFGL 2688

AFGL 2688 (the "Egg Nebula") is a bipolar reflection nebula (Ney et al. 1975) at visible and near-infrared wavelengths. It has a central star that exhibits the spectrum of a carbon-rich supergiant (Crampton et al. 1975; Lo & Bechis 1976). Similar in visible appearance to AFGL 915, each lobe shows two "jets" or "horns" extending away from the central region (Crampton et al. 1975; Latter et al. 1993; Sahai et al. 1998a). The lobes have identical spectra at visible wavelengths, but their brightness differs significantly (Cohen & Kuhi 1977). The near-IR spectrum is dominated by H_2 rotation-vibration lines (Thronson 1982; Beckwith 1984; Latter et al. 1993). A central source is seen in the mid-IR and longer wavelengths, with fainter extended emission along the axis of the nebula (Hora et al. 1996). There is an enigmatic equatorial region seen in H_2 emission and might be traced by other molecular species, such as HCN (Latter et al. 1993; Bieging & Ngyuen-Quang-Rieu 1996; Sahai et al. 1998b).

Similar to AFGL 618, this object also has a rich molecular content. SiC_2 is seen in absorption (Cohen & Kuhi 1977); this feature is usually found in stars of the highest carbon abundance. Strong absorption features of C_3 and emission in C_2 (Crampton et al. 1975) are present, while C_2 is also seen in absorption in reflected light from the lobes (Bakker et al. 1997). The CO $J = 1 \rightarrow 0$ line shows three distinct velocity structures (Kawabe et al. 1987; Young et al. 1992).

Our results for this object from this survey were previously presented in Hora & Latter (1994, 1995) and our narrowband imaging in Latter et al. (1993). The spectra are reproduced here for comparison with the rest of the survey. Spectra were obtained at several positions in the nebula, including positions along the N lobe, and in the equatorial region (see Hora & Latter 1994 for details). The emission is segregated; the core is dominated by continuum emission, there are emission lines from C_2 and CN further from the core along the lobes, and the H_2 emission is confined to the ends of the lobes and in the equatorial region in what appears to be a ring or toroidal structure (Latter et al. 1993; Sahai et al. 1998b). Our analysis of the H_2 line ratios showed that the emission is collisionally excited in shocks, with no discernible difference between the emission in the lobes and the equatorial region.

3.4. Continuum - dominated

These are young PNe or PPNe that have strong warm dust continuum and little line emission. The strongest component is in general the core, with most of the emission from an unresolved point source. In some of the nebulae, emission structure extends a few arcseconds from the core region. Also, in objects such as AFGL 915, they are associated with larger optical nebulae that extend arcminutes from the core. In this survey we have sampled only the regions near the core.

3.4.1. AFGL 915

AFGL 915 (the "Red Rectangle") is a carbon-rich biconical reflection nebula with a metal-depleted spectroscopic binary at its center (Cohen et al. 1975). The nebula appears axially symmetric and shows spikes running tangent to the edge of the bicone. Surrounding the post-AGB star at its center is a circumbinary disk viewed edge-on (Jura, Balm, & Kahane 1995) which could be oxygen-rich (Waters et al.

4.1.2. *The Carbon-to-Oxygen Ratio*

Carbon stars, although a small fraction of all AGB stars, return about half of the total mass injected into the ISM by all AGB stars, since they have on average much higher mass loss rates ($> 10^{-4} M_{\odot}\ yr^{-1}$) than do O-rich objects. The carbon-to-oxygen (C/O) abundance ratio in PNe has previously been shown to correlate with morphology (Zuckerman & Aller 1986), with bipolar PNe tending to be carbon-rich. It is therefore expected that the C/O ratio also correlates with the spectral classifications presented here. This is in general the case, with the H I - line dominated PNe having C/O ratios less than or about 1, whereas the remaining categories which are dominated by the bipolar PNe have C/O ratios >1, as reported by Zuckerman & Aller (1986) and Rola & Stasińska (1994). Rola & Stasińska discuss problems with previous determinations of the C/O ratio, and use different criteria that result in a slightly lower percentage of carbon-rich PNe (35%) than others. We use their ratios in the discussion below.

The morphology of PN also has been shown to depend on the progenitor mass (see Corradi & Schwarz 1995), with the bipolar PN being more massive than other morphological types. This relationship, along with the link between carbon abundance and morphology, suggests that carbon stars are the projenitors of bipolar PN and those with a large amount of molecular material. The mechanisms that cause massive carbon-rich stars to preferentially form bipolar PN are still not understood.

There are some exceptions to the correlation of morphological type to C/O ratio; in particular, NGC 6543 has a much higher value (9.55) than the others in the class. In the other extreme, NGC 2346 stands out as having a low C/O ratio (0.35) compared to other bipolar PNe in the H_2 - dominated group. This object is a much more evolved object than the others in its group (e.g., AFGL 2688), and exhibits weak Paβ emission, showing that the ionized gas is present although weak relative to the molecular emission in the nebula.

4.2. Summary of Molecular Hydrogen Emission in PNe

A long standing problem in the interpretation of H_2 emission from interstellar and circumstellar environments is understanding the excitation mechanism. Three fundamental mechanisms are possible. One is excitation of a near-infrared fluorescence spectrum resulting from a rotational-vibrational cascade in the ground electronic state following electronic excitation by the absorption a UV photon in the Lyman and Werner bands (Black & van Dishoeck 1987). The second excitation mechanism is collisional excitation in a warm gas ($T_K \gtrsim 1600$ K). While UV excitation in a low density gas produces an easily identifiable spectrum, the level populations can be driven to produce thermal line ratios when the UV flux is large and densities begin to exceed $\approx 10^4$ cm^{-3} (Sternberg & Dalgarno 1989). Detailed spectral and morphological analysis are often required to determine an origin of the near-IR spectrum. The third excitation mechanism is formation of H_2 on the surfaces of dust grains and in the gas phase. While potentially important in isolated regions of certain objects, we do not consider this to be generally important in PNe and PPNe relative to the other two processes. This is because molecular formation in PNe is relatively slow compared to dissociation rates.

In PNe and PPNe, the situation can be complicated by both dominant excitation mechanisms being present simultaneously, and in different forms. Several ways of exciting near-IR emission from H_2 have been identified as possible: direct thermal excitation in warm gas created behind moderate velocity shockwaves, direct excitation by UV photons from the hot central star, somewhat indirectly by collisional excitation in warm gas created by rapid grain streaming (e.g. Jura & Kroto 1990), and excitation through absorption of Lyα photons (by an accidental resonances with the $B^1\Sigma_u^+ - X^1\Sigma_g^+$ $v = 1 - 2$ P(5) and R(6) transitions of H_2) which can be generated in a nearby strong shock (e.g., Black & van Dishoeck 1987).

The first two mechanisms have been clearly identified in several PNe, such as thermal excitation in AFGL 2688 (e.g., Hora & Latter 1994; Sahai et al. 1998a), pure UV excitation in a low density gas around Hb 12 (e.g., Dinerstein et al. 1988; Hora & Latter 1996; Luhman & Rieke 1996), and UV excitation in a high density gas in M 2-9 (Hora & Latter 1994) and NGC 7027 (Graham et al. 1993b; this paper). A combined spectrum was found from a detailed analysis of AFGL 618 (Latter et al. 1992; this paper). While the form of the excitation might be clear for these and other objects, it is not always evident what is the source of the warm gas or UV photons. Winds are present in AFGL 2688 which could directly shock heat the gas, but considerable grain streaming is likely

We thank Xander Tielens and David Hollenbach for useful discussions and encouragement. We acknowledge support from NASA grant 399-20-61 from the Long Term Space Astrophysics Program. WBL was supported during part of this study by a National Research Council Research Associateship.

REFERENCES

Aaquist, O. B., & Kwok, S. 1990, A&AS, 84, 229

Acker, A., Marcout, J., Ochsenbein, F., Scholn, C., Stenholm, B., & Tylenda, R. 1992, The Strasbourg-ESO Catalogue of Galactic Planetary Nebulae (München: ESO)

Aspin, C. et al. 1993, A&A, 278, 255

Bachiller, R., Fuente, A., Bujarrabal, V., Colomer, F., Loup, C., Omont, A., & de Jong, T. 1997, A&A, 319, 235

Bakker, E.J., van Dishoeck, E.F., Waters, L.B.F.M., & Shoenmaker, T. 1997, A&A, 323, 469

Balick, B. 1987, AJ, 94, 671

Balick, B., Bignell, C. R., Hjellming, R. M., & Owen, R. 1987, AJ, 94, 948

Balick, B., Gonzalez, G., Frank, A., & Jacoby, G. 1992, ApJ, 392, 582

Balick, B., Alexander, J., Hajian, A. R., Terzian, Y., Perinotto, M., & Patriarchi, P. 1998, AJ, 116, 360

Barker, T. 1991, ApJ, 371, 217

Beckwith, S., Beck, S.C., & Gatley, I. 1984, ApJ, 280, 648

Bieging, J. H. & Ngyuen-Quang-Rieu 1996, AJ, 112, 706

Black, J. H., & van Dishoeck, E. F. 1987, ApJ, 322, 412

Bohigas, J., & Olguin, L. 1996, RMxAA, 32, 47

Bowers, C. W., Blair, W. P., Long, K. S., & Davidsen, A. F. 1995, ApJ, 444, 748

Bregman, J. D., Rank, D., Temi, P., Hudgins, D., & Kay, L. 1993, ApJ, 411, 794

Bryce, M., Balick, B., & Meaburn, J. 1994, MNRAS, 266, 721

Bujarrabal, V., Alcolea, J., & Planesas, P. 1992, A&A, 257, 701

Carsenty, U., & Solf, J. 1982, A&A, 106, 307

Cernicharo, J., Guelin, M., Martin-Pintado, J., Denalver, J.,& Maversberger, R. 1989, A&A, 222, L1

Cohen, M., & Barlow, M. J. 1974, ApJ, 193, 401

Cohen, M. & Jones, B. F. 1987, ApJ, 321, L151

Cohen, M. & Kuhi, L.V. 1977, ApJ, 213, 79

Cohen, M., et al. 1975, Ap.J. 196, 179

Corradi, R. L. M., & Schwarz, H. E. 1995, A&A, 293, 871

Crampton, D., Cowley, A.P., & Humphreys, R.M. 1975, ApJ, 198, L135.

Cuesta, L., Phillips, J. P., & Mampaso, A. 1996, A&A, 313, 243

Dayal, A. & Bieging, J.H. 1996, Ap.J. 472, 703

Dayal, A., Sahai, R., Trauger, J., Hora, J. L., Fazio, G. G., Hoffmann, W. F., Bieging, J. H., Deutsch, L. K., & Latter, W. B. 1997, BAAS, 191, 1509

Dinerstein, H. L., Carr, J. S., Harvey, P. M., & Lester, D. F. 1986, in Summer School on Interstellar Processes (Abstract book), p. 43

Dinerstein, H. L., Lester, D. F., Carr, J. S., & Harvey, P. M. 1988, ApJ, 327, L27

Dinerstein, H. L., & Crawford, J. 1998, in Proc. IAU Symp. 180, in press

Feibelman, W. A., Hyung, S., & Aller, L. H. 1996, MNRAS, 278, 625

Feibelman, W. A. 1997, ApJS, 109, 481

Garcia-Lario, P., Manchado, A., Suso, S. R., Pottasch, S. R., & Olling, R. 1990, A&AS, 82, 497

Geballe, T. R., Burton, M. G., & Isaacman, I. 1991, MNRAS, 253, 75

Gillett, F. C., Merrill, K. M., & Stein, W. A. 1972, ApJ, 172, 367

Glinski, R.J., Lauroesch, J.T., Reese, M.D., & Sitko, M.L. 1997, Ap.J. 490, 826

Goodrich, R. W. 1991, ApJ, 376, 654

Graham, J. R., Serabyn, E., Herbst, T. M., Matthews, K., Neugebauer, G., Soifer, B. T., Wilson, T. D., & Beckwith, S. 1993, AJ, 105, 250

Graham, J. R., Herbst, T. M., Matthews, K., Neugebauer, G., Soifer, T., Serabyn, E., & Beckwith, S. 1993b, ApJ, 408, L105

Greaves, J.S. & Holland, W.S. 1997, A&A, 327, 342

Persi, P., Preite Martinez, A., Ferrari-Toniolo, M., & Spinoglio, L. 1987, in Planetary and protoplanetary nebulae: From IRAS to ISO (Dordrecht, D. Reidel), 221

Phillips, J. P., & Cuesta, L. 1996, AJ, 111, 1227

Ramsay, S. K., Chrysostomou, A., Geballe, T. R., Brand, P. W. J. L., & Mountain, M. 1993, MNRAS, 263, 695

Rao, K. N., Humphreys, C. J., & Rank, D. H. 1966, Vacuum Wavelengths in the Infrared (New York: Academic Press, Inc.)

Reay, N. K., Atherton, P. D., & Taylor, K. 1983, MNRAS, 203, 1087

Rieke, G. H., & Lebofsky, M. J. 1985, ApJ, 288, 618

Rola, C., & Stasińska, G. 1994, A&A, 282, 199

Rudy, R. J., Rossano, G. S., Erwin, P. & Puetter, R. C. 1991, ApJ, 368, 468

Rudy, R. J., Erwin, P., Rossano, G. S., & Puetter, R. C. 1992, ApJ, 384, 536

Sahai, R., Wootten, A., Schwarz, H. E., & Wild, W. 1994, ApJ, 428, 237

Sahai, R., et al. 1998a, ApJ, 493, 301

Sahai, R., et al. 1998b, ApJ, 492, 163

Schmidt, G. D., Cohen, M., & Margon, B. 1980, Ap.J. 239, L133

Schwarz, H. E., Corradi, R. L. M., & Melnick, J. 1992, A&AS, 96, 23

Scrimger, M. J., Lowe, R. P., Moorhead, J. M., & Wehlau, W. H. 1978, PASP, 90, 257

Shibata, K. M., Tamura, S., Deguchi, S., Hirano, N., Kameya, O., & Kasuga, T. 1989, ApJ, 345, L55

Shupe, D. L., Armus, L., Matthews, K., & Soifer, B. T. 1995, ApJ, 109, 1173

Shupe, D. L., Larkin, J. E., Knop, R. A., Armus, L., Matthews, K, & Soifer, B. T. 1998, ApJ, 498, 267

Smith, H. A., Larson, H. P., & Fink, U. 1981, ApJ, 244, 835

Sternberg, A., & Dalgarno, A. 1989, ApJ, 338, 197

Thronson, H.A. 1981, ApJ, 248, 984

Thronson, H.A. 1982, AJ, 87, 1207

Thronson, H.A. 1983, ApJ, 264, 599

Trammell, S. R., Dinerstein, H. L., & Goodrich, R. W. 1993, ApJ, 402, 249

Treffers, R. R., Fink, U., Larson, H. P., & Gautier III, T. N. 1976, ApJ, 209, 793

Walsh, J. R., Meaburn, J., & Whitehead, M. J. 1991, A&A, 248, 613

Waters, L.B.F.M., et al. 1998, Nature 391, 868

Wiese, W. L., Smith, M. W., & Miles, B. M. 1969, Nat. Stand. Ref. Data Ser., Nat. Bur. Stand. (US), 22, 189

Willner, S. P., Jones, B., Puetter, R. C., Russell, R. W., & Soifer, B. T. 1979, ApJ, 234, 496

Westbrook, W. E., Becklin, E. E., Merrill, K. M., Neugebauer, G., Schmidt, M., Willner, S. P., & Wynn-Williams, C. G. 1975, ApJ, 202, 407

Whitelock, P. A. 1985, MNRAS, 213, 59

Young, K., Serabyn, G., Phillips, T.G., Knapp, G.R., Gusten, R., & Schultz, A. 1992, ApJ, 385, 265

Young K. 1997, ApJ, 488, L157

Zhang, C. Y., & Kwok, S. 1992, ApJ, 385, 255

Zhang, C. Y., & Kwok, S. 1998, ApJS, 117, 341

Zuckerman, B., & Gatley, I. 1988, ApJ, 324, 501

This 2-column preprint was prepared with the AAS LaTeX macros v4.0.

Fig. 13.— M 4-18 (see caption to Figure 1).

Fig. 14.— Spectra of NGC 40 and NGC 2440. The spectra have been offset and scaled by the constants shown in the plot labels. At the bottom, some of the prominent lines have been labeled with small vertical lines. The first row are H I, the second row He I, and the third row H_2. Below the rows individual lines have been indicated. The positions in the nebula where these spectra were taken is given in Table 1.

Fig. 15.— NGC 2440 (see caption to Figure 14).

Fig. 16.— NGC 6720 (see caption to Figure 14).

Fig. 17.— NGC 7026 (see caption to Figure 14).

Fig. 18.— NGC 7027 (see caption to Figure 14).

Fig. 19.— BD+30°3639 (see caption to Figure 14).

Fig. 20.— Hubble 12 (see caption to Figure 14).

Fig. 21.— IC 2003 and IRAS 21282+5050 (see caption to Figure 14).

Fig. 22.— M 1-16 (see caption to Figure 14).

Fig. 23.— M 1-92 (see caption to Figure 14).

Fig. 24.— M 2-9 (see caption to Figure 14).

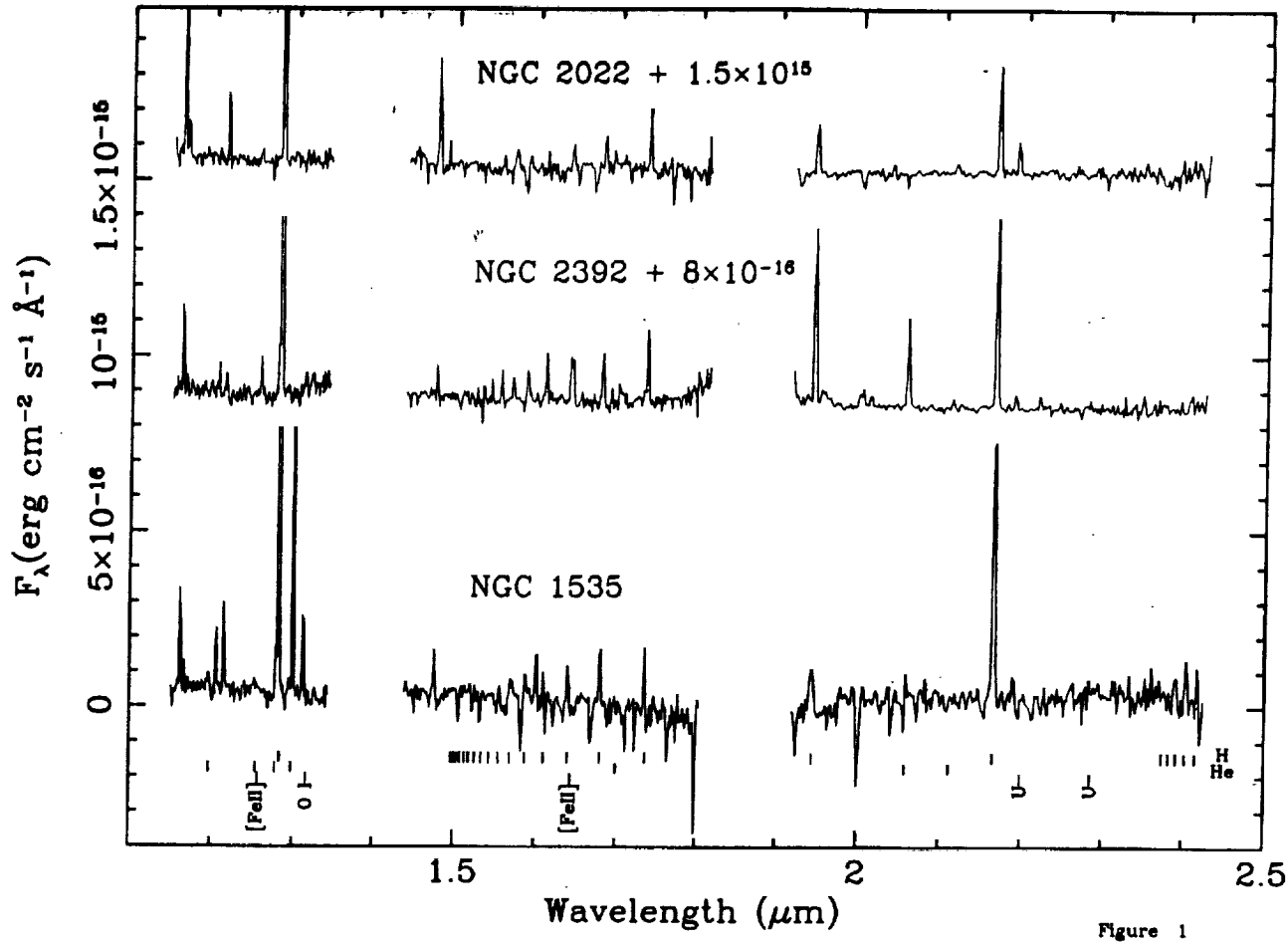

Figure 1

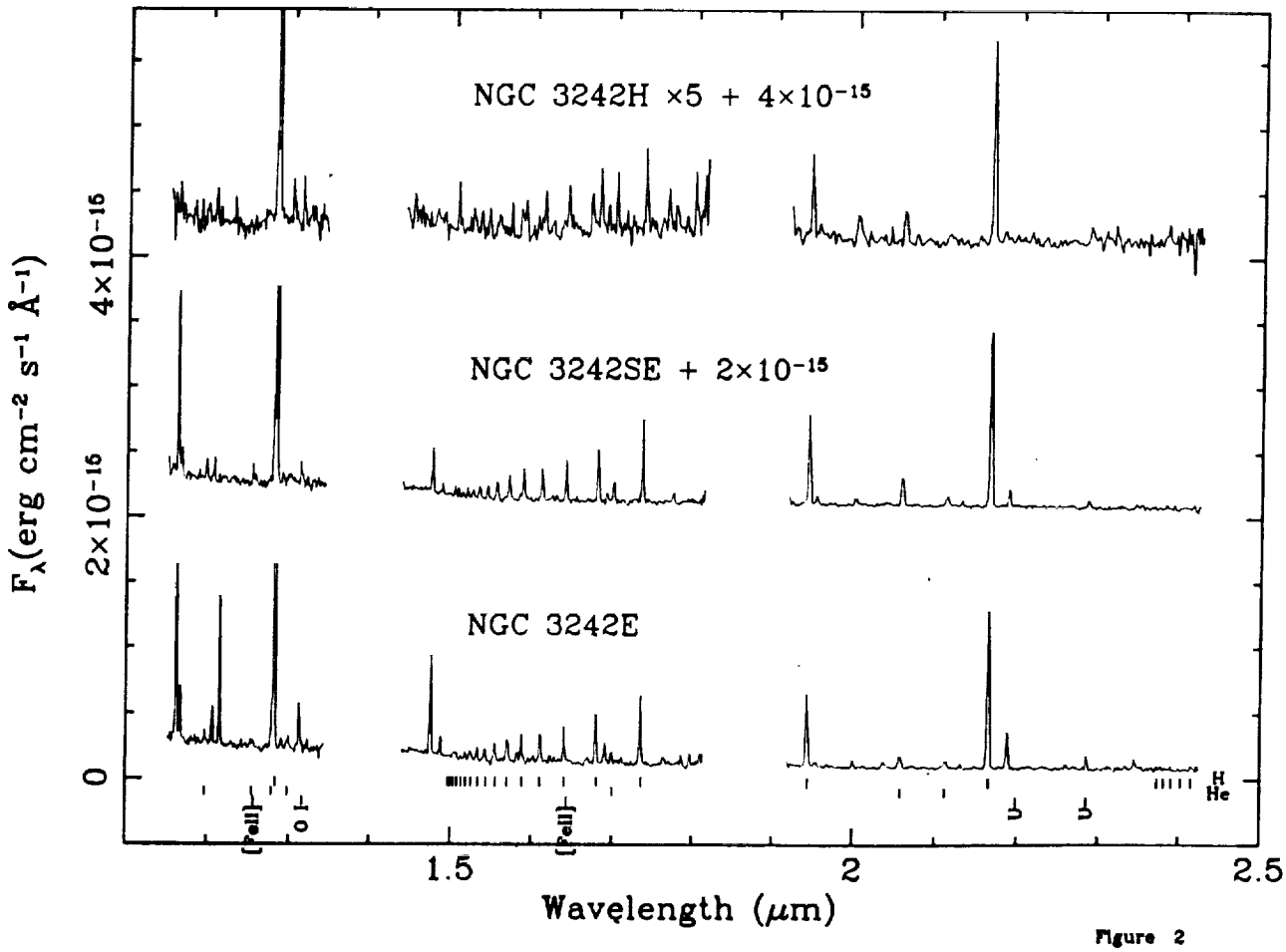

Figure 2

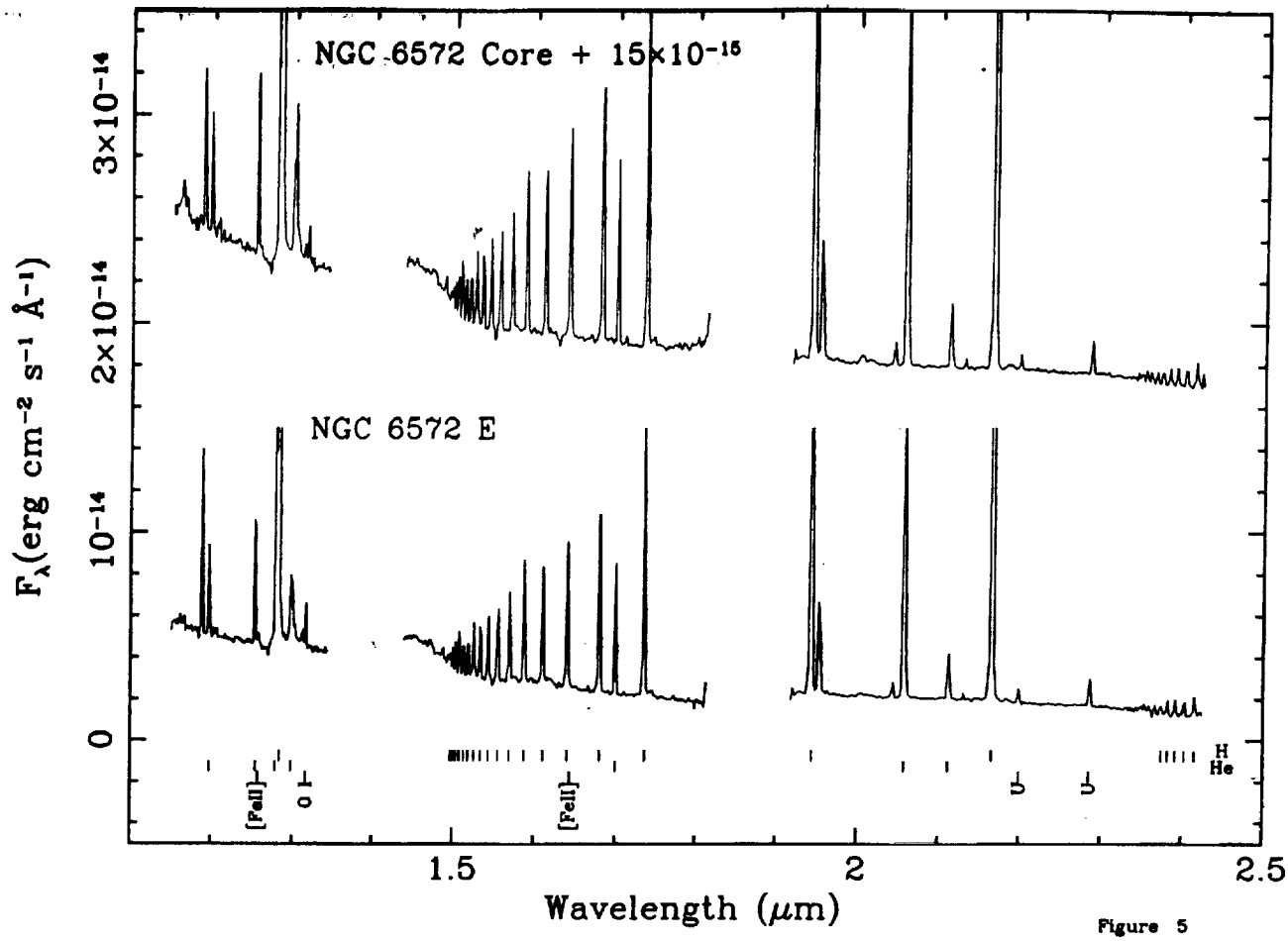

Figure 5

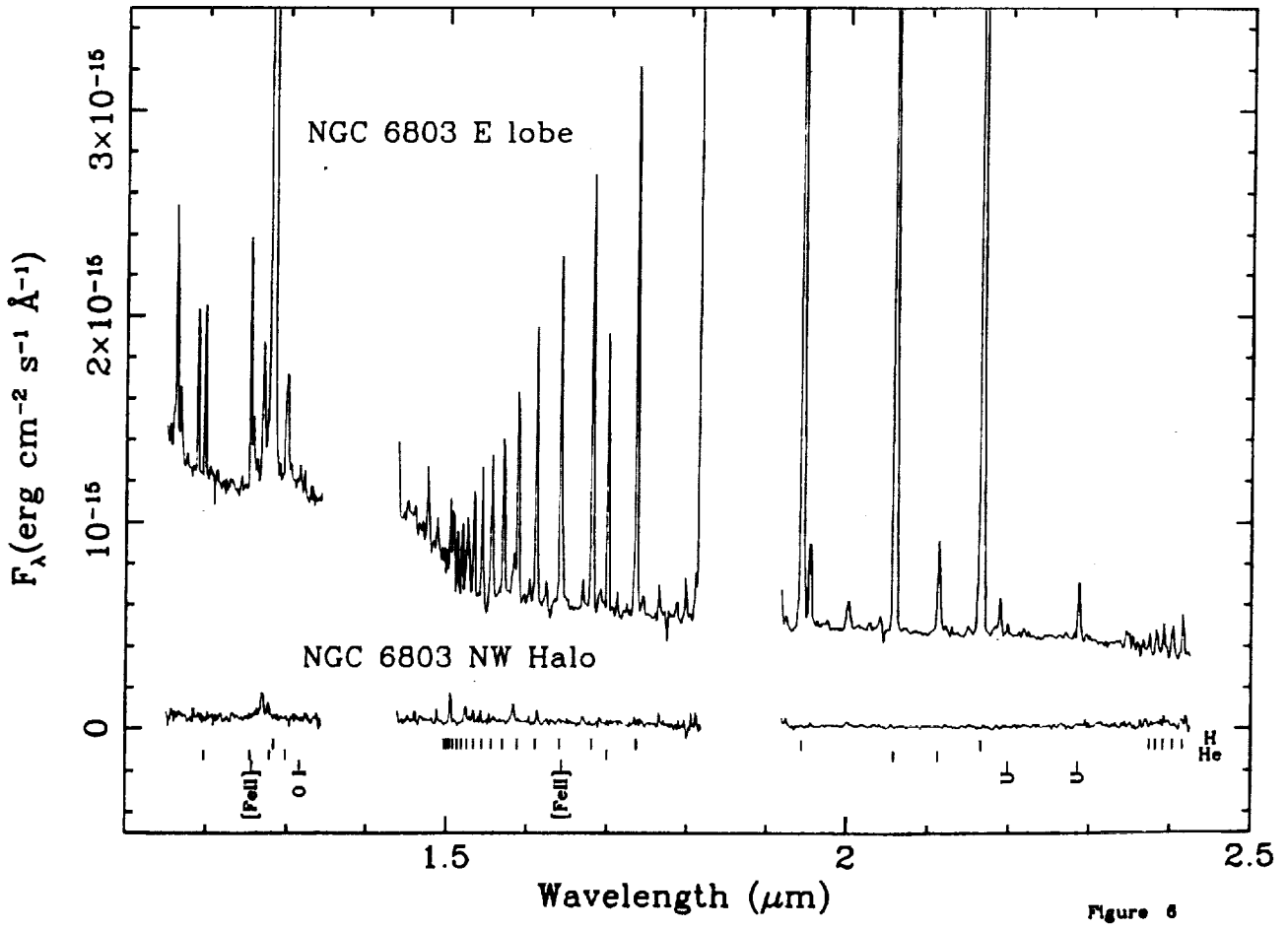

Figure 6

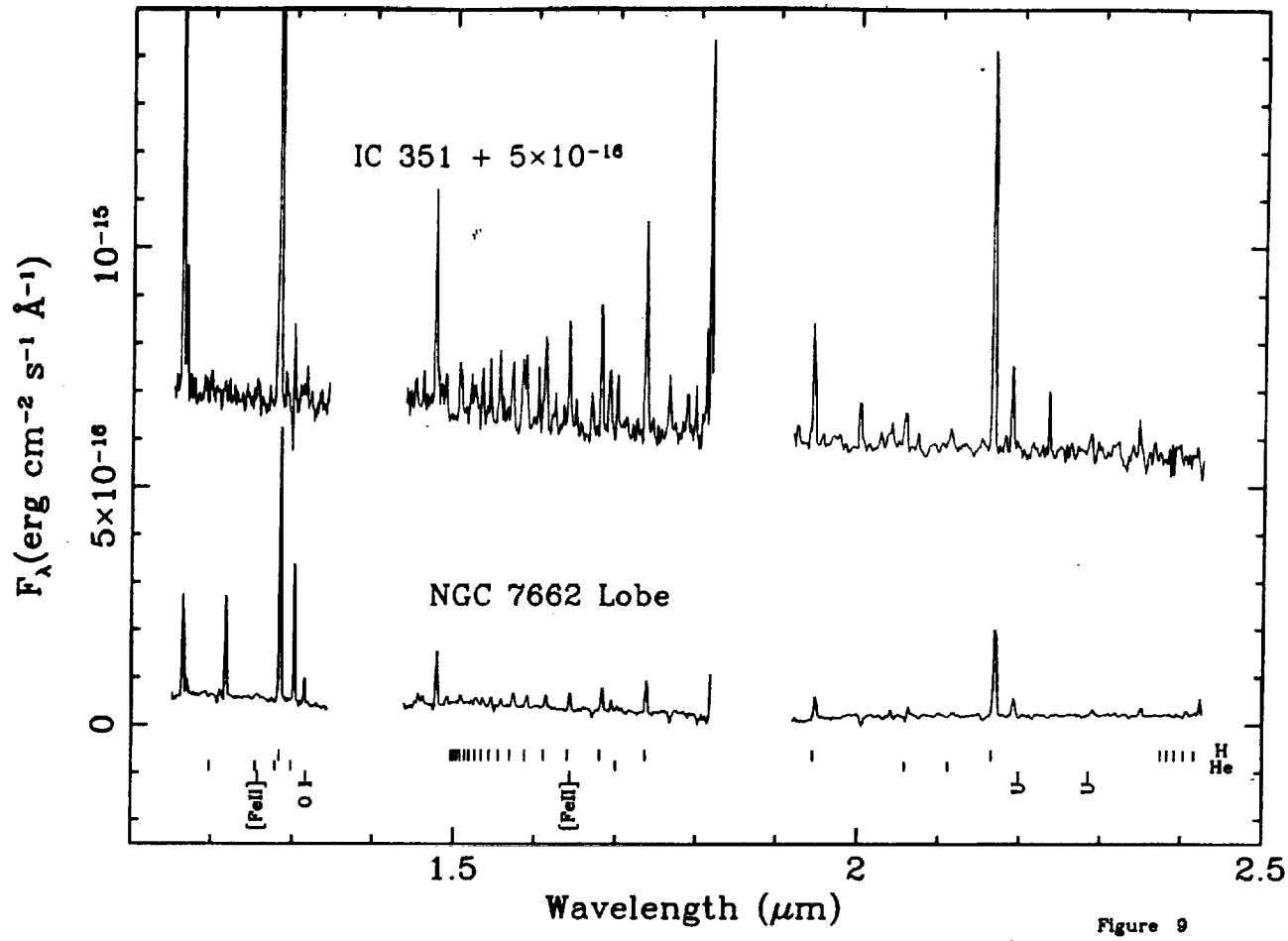

Figure 9

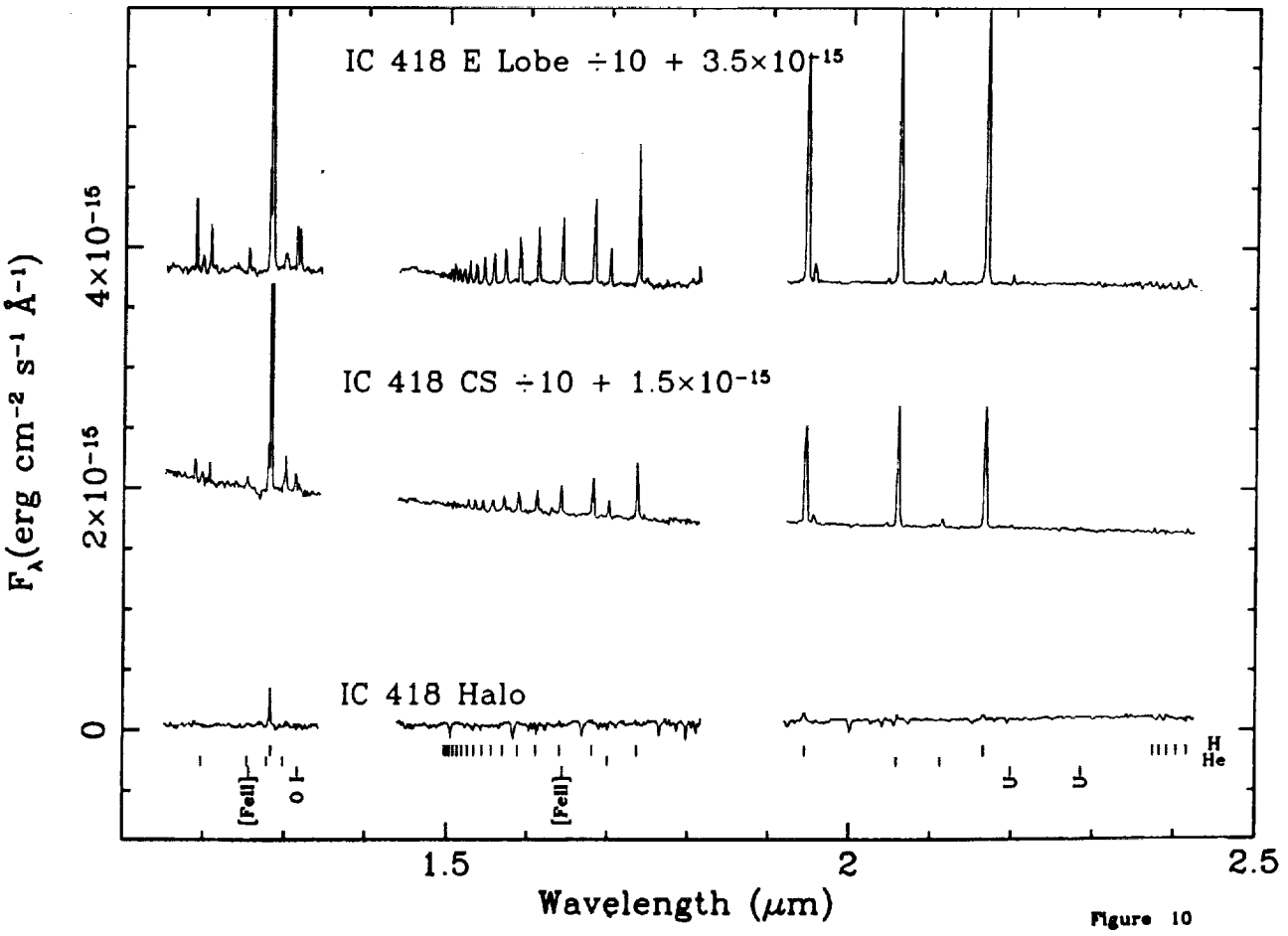

Figure 10

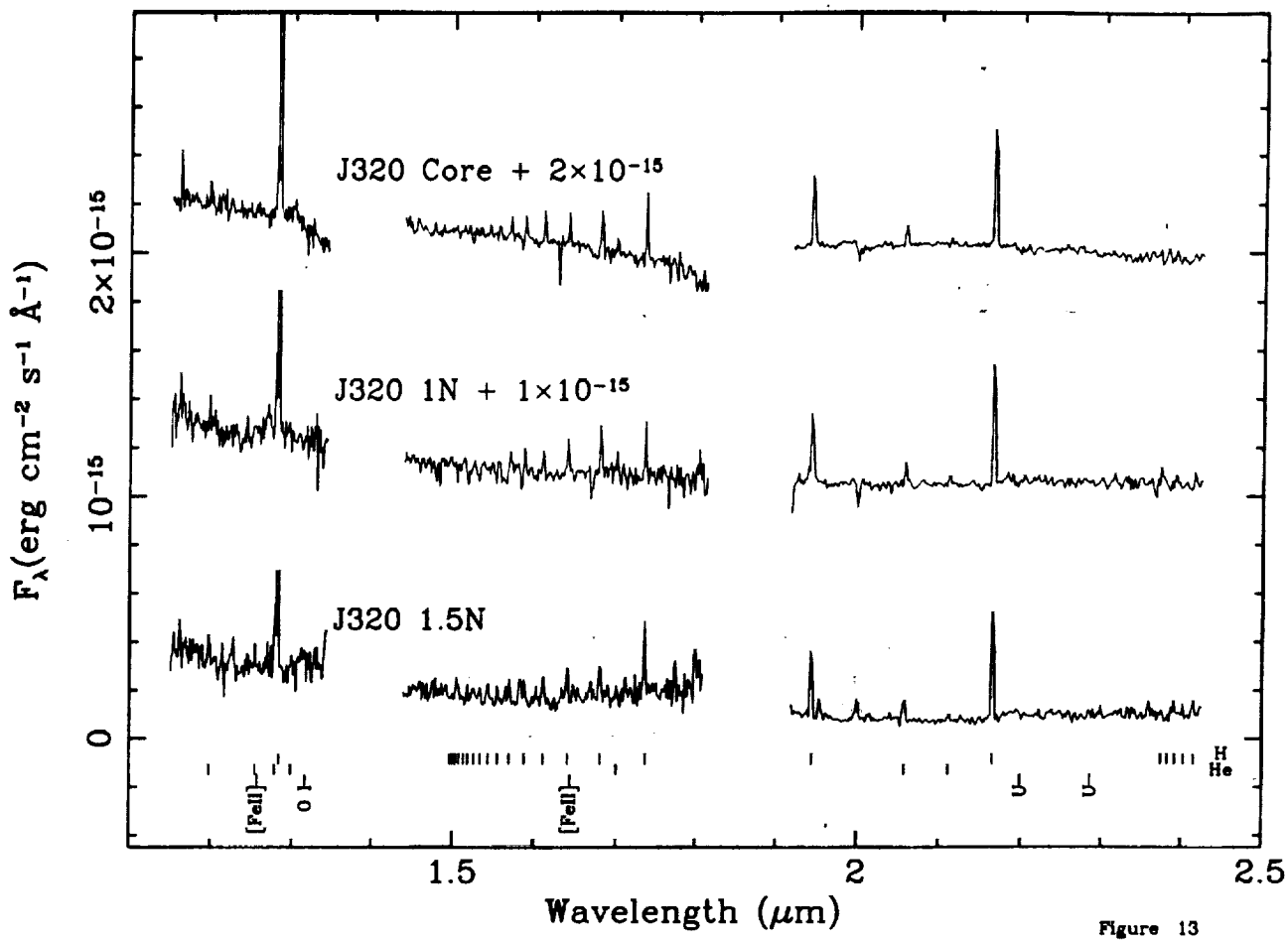

Figure 13

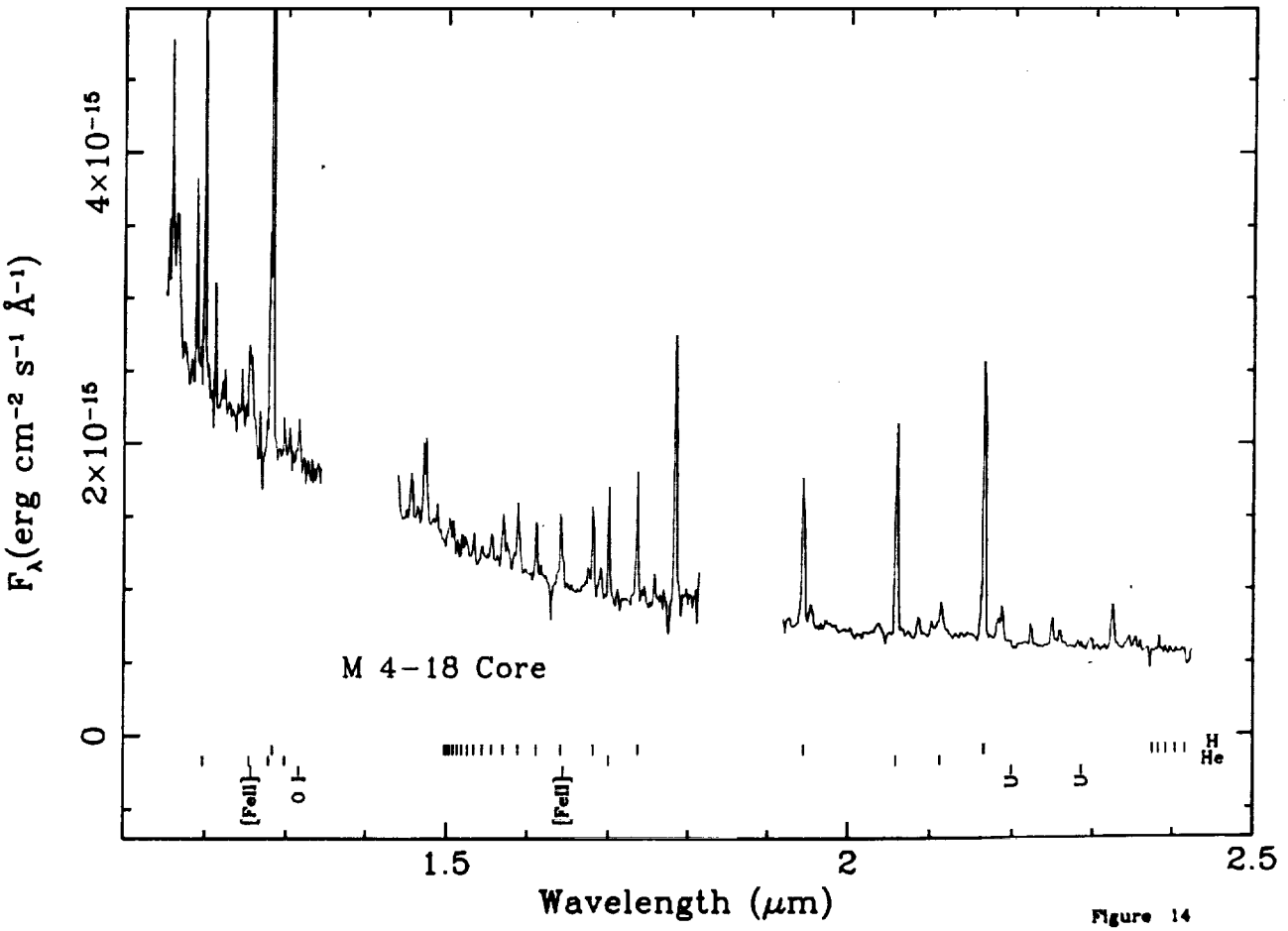

Figure 14

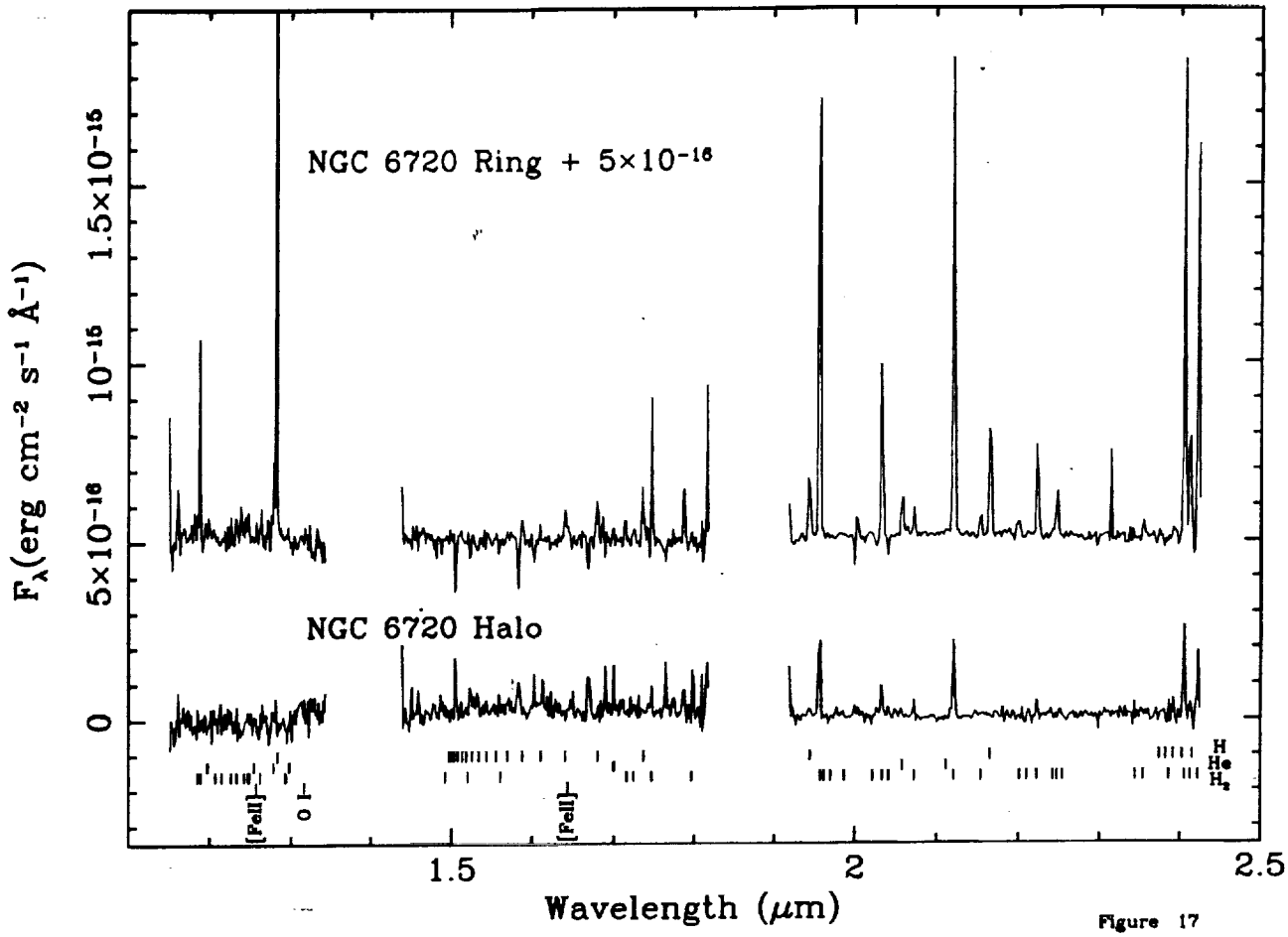

Figure 17

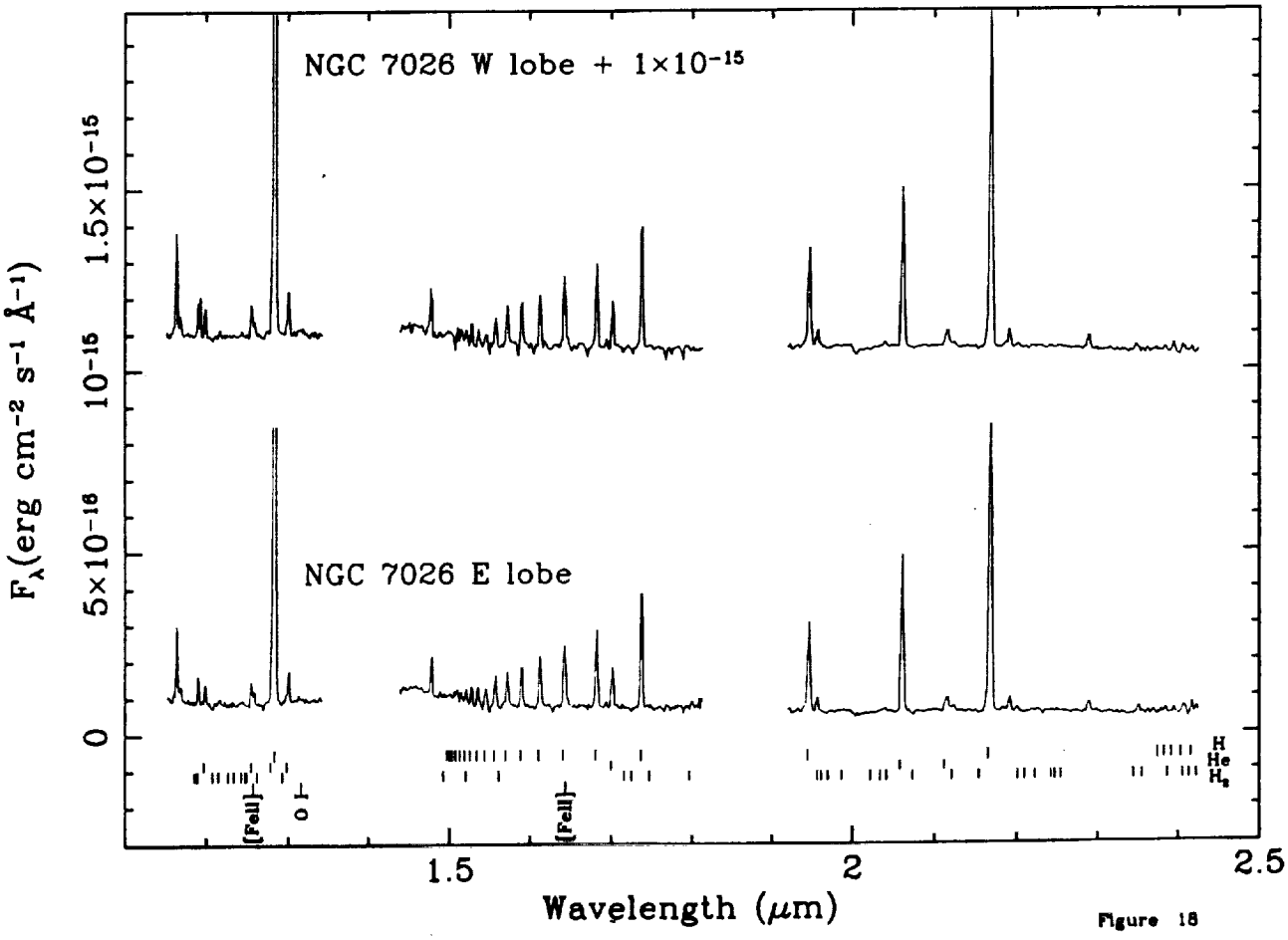

Figure 18

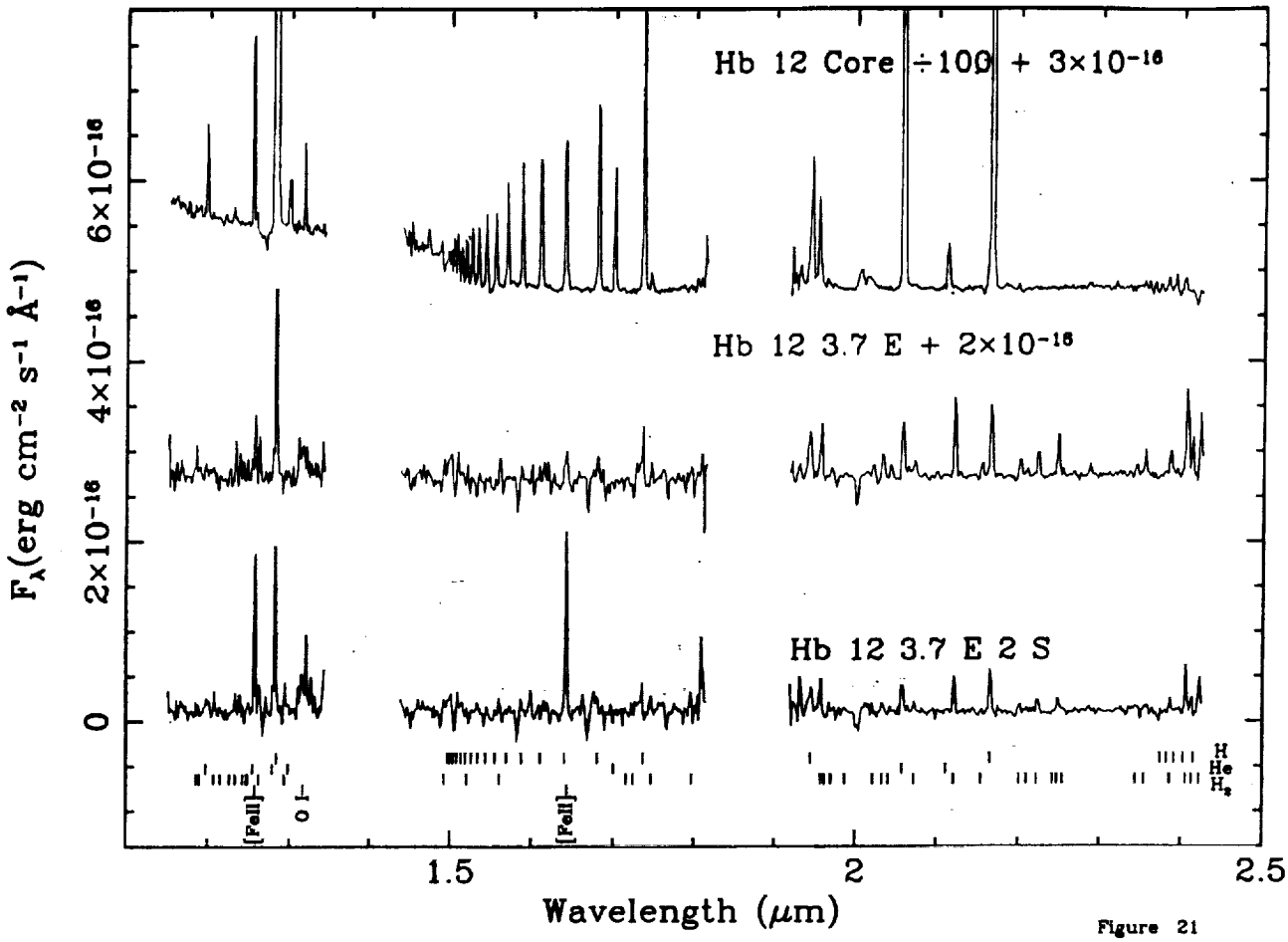

Figure 21

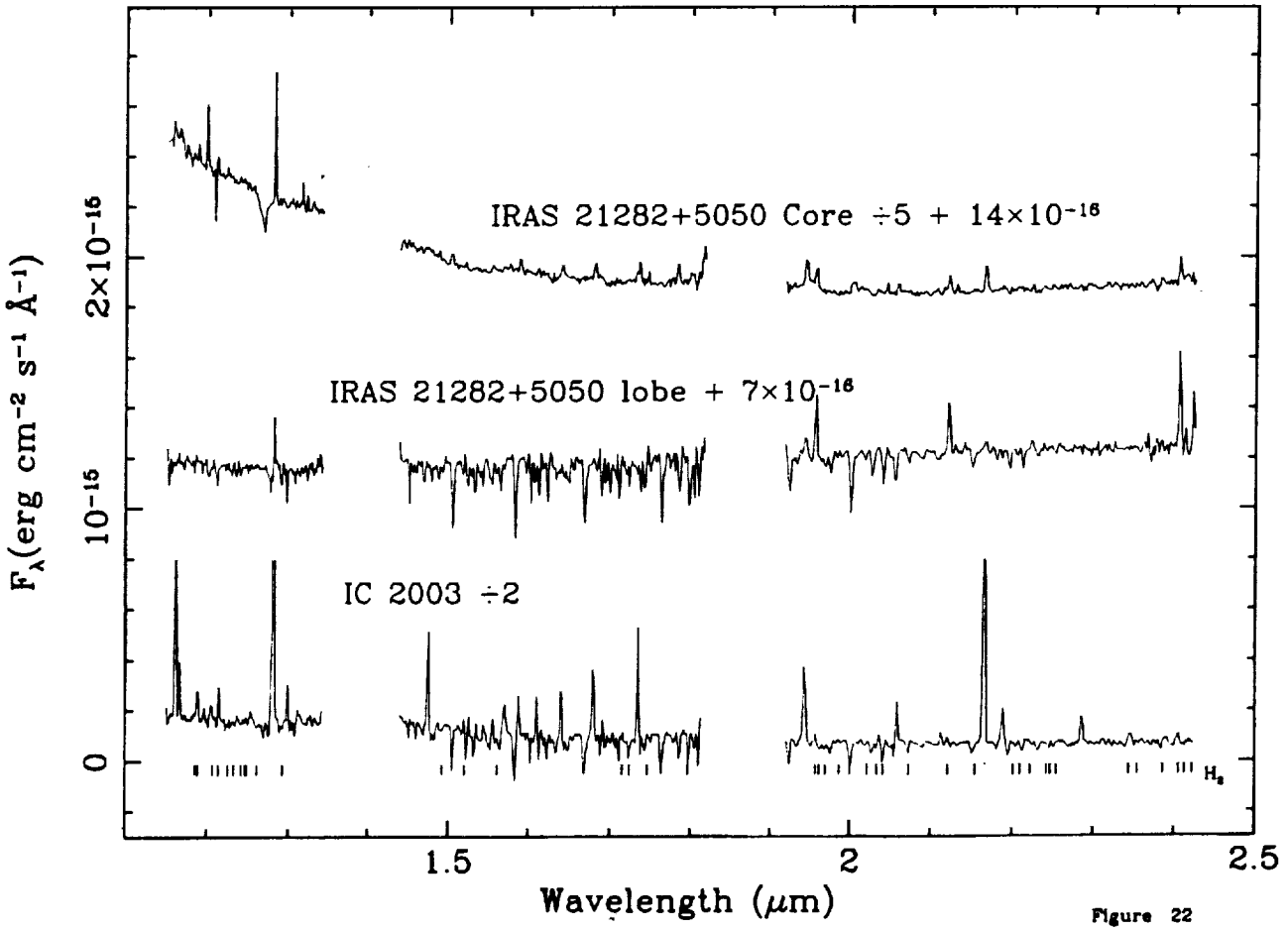

Figure 22

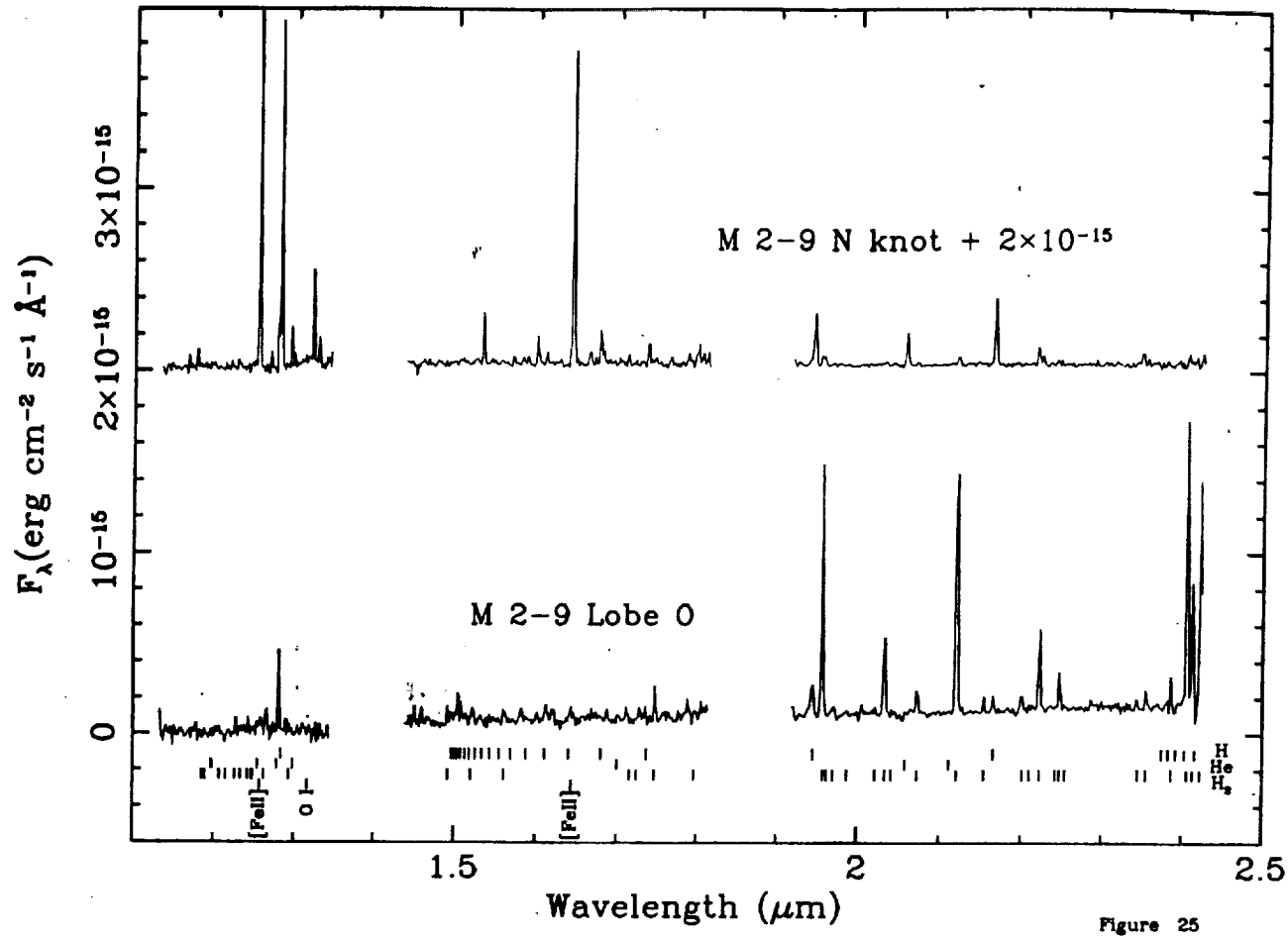

Figure 25

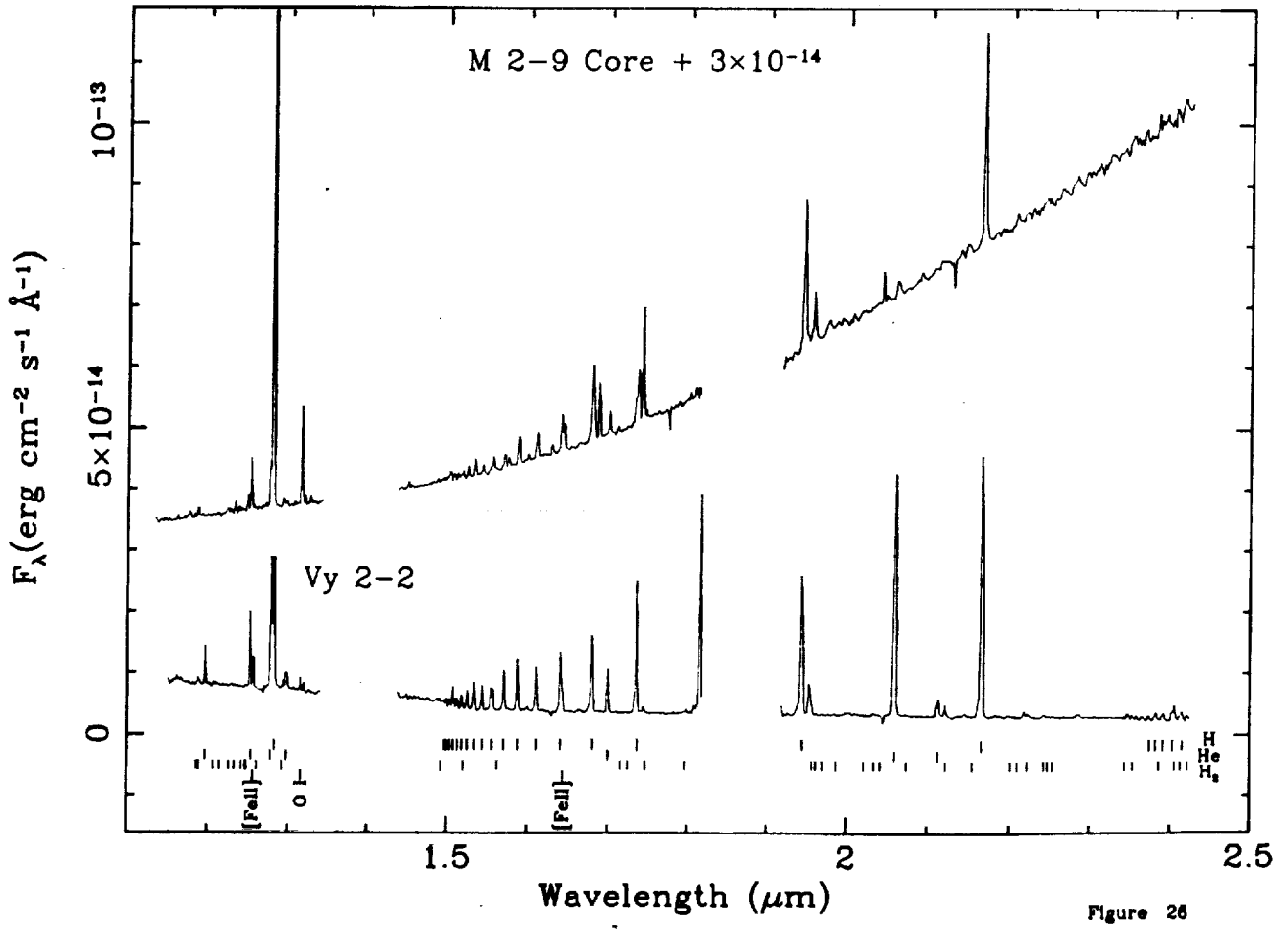

Figure 26

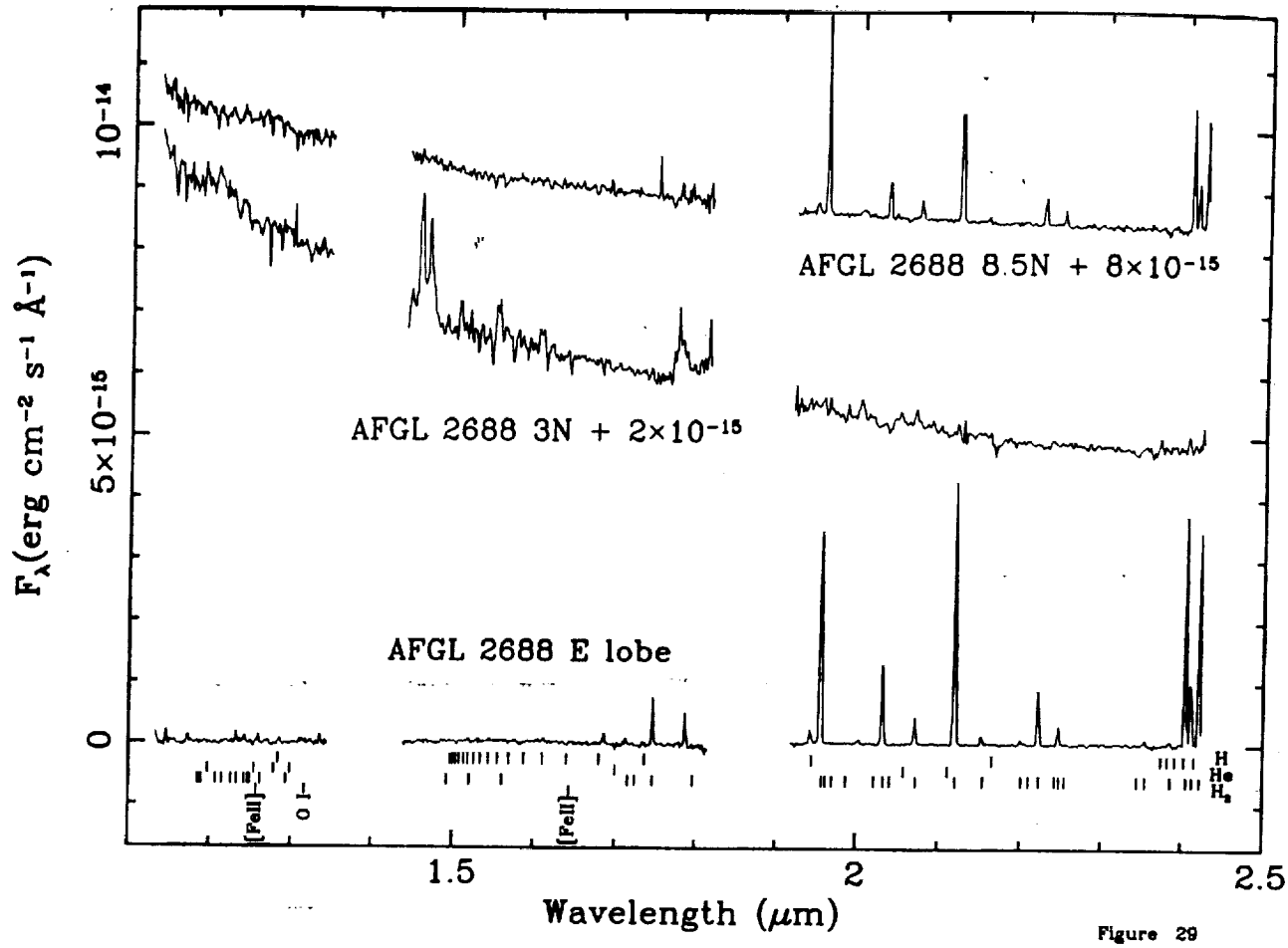

Figure 29

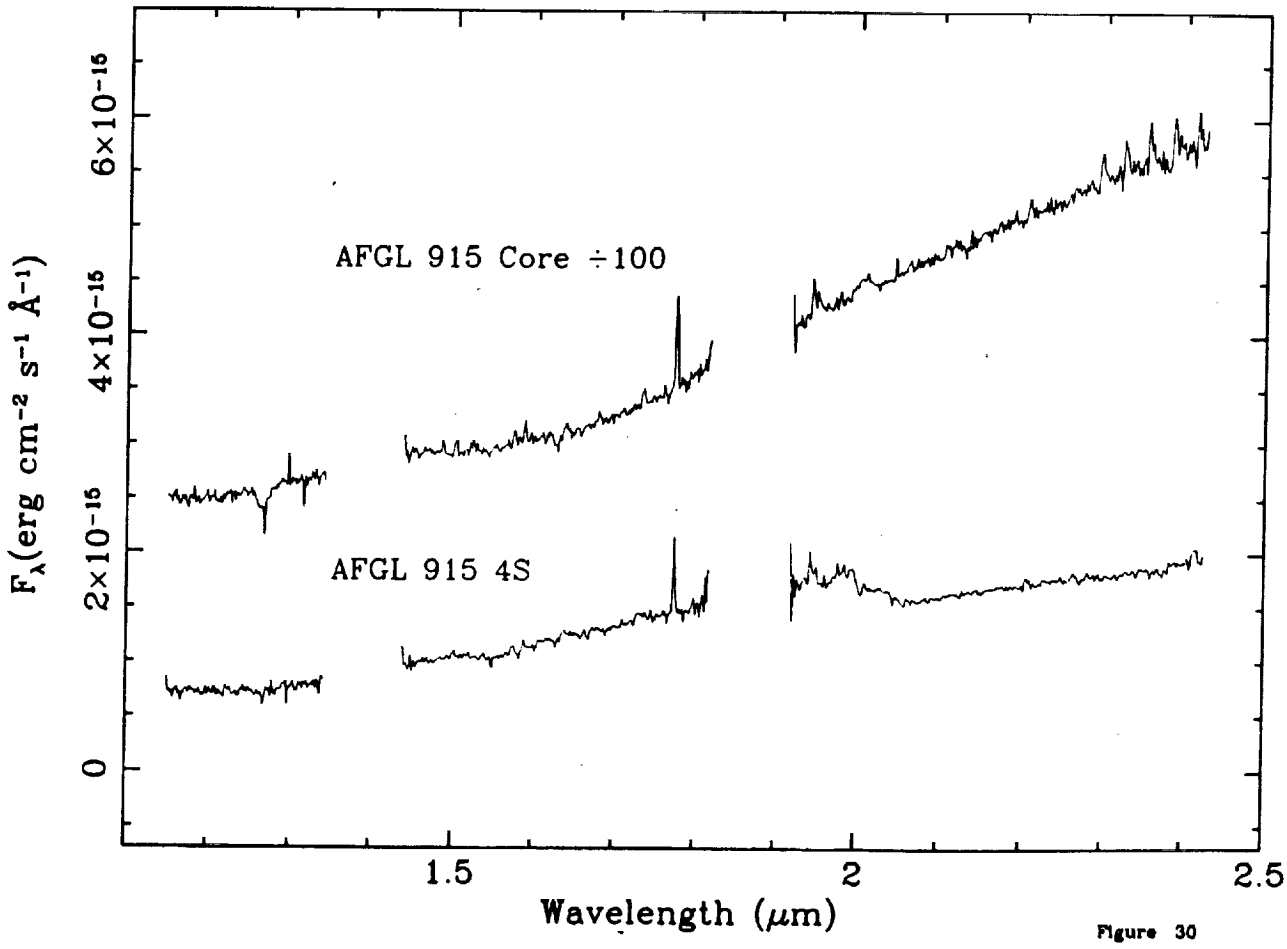

Figure 30

Figure 33a

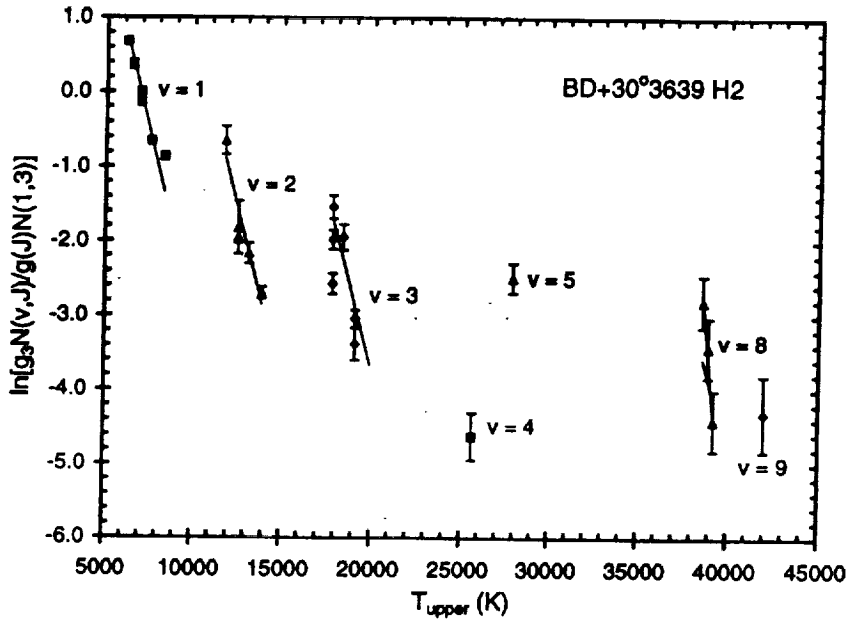

Figure 33b

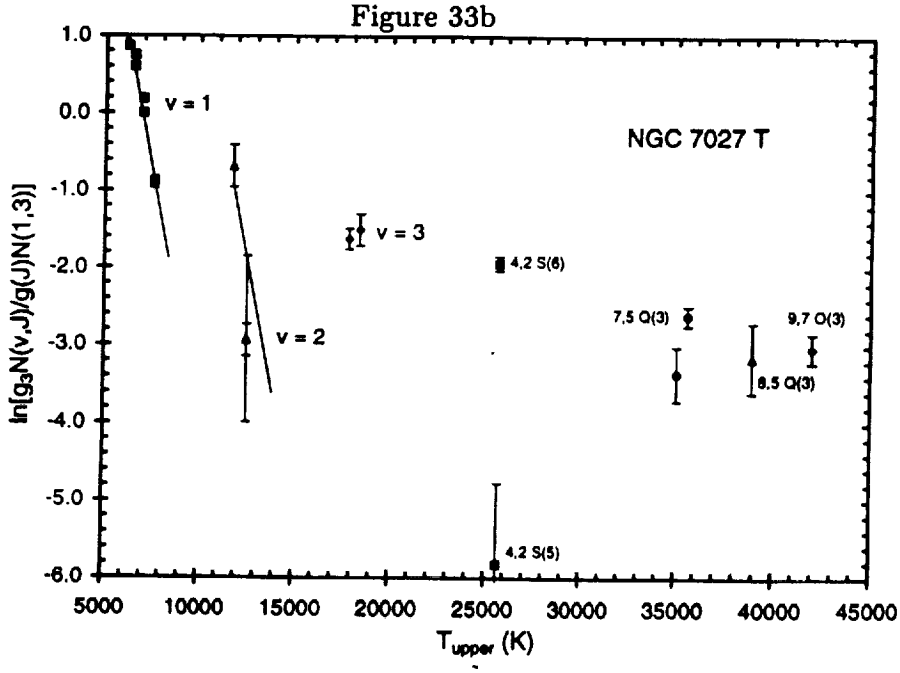

Figure 33e

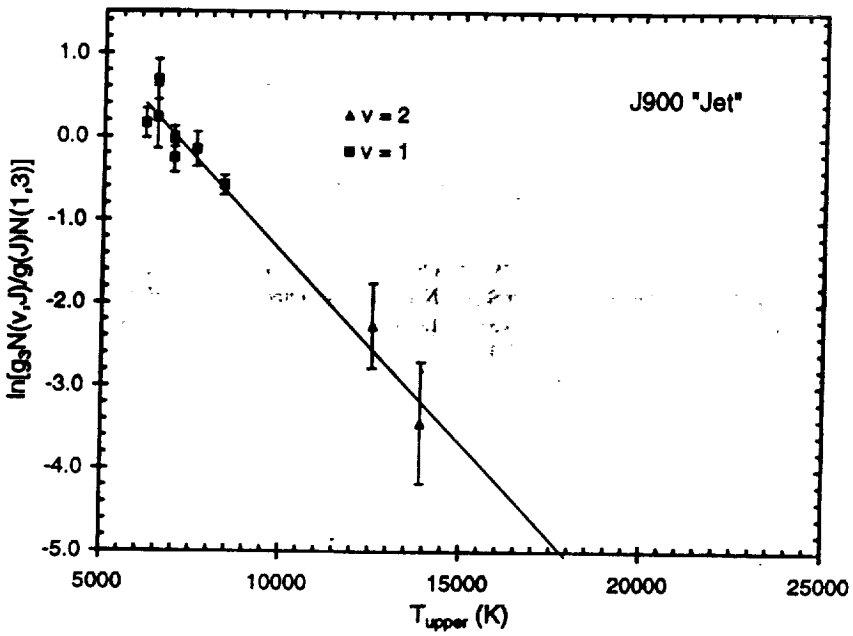
J900 "Jet"
▲ v = 2
■ v = 1
ln[g_S N(v,J)/g(J)N(1,3)]
1.0
0.0
-1.0
-2.0
-3.0
-4.0
-5.0
5000
10000
15000
20000
25000
T_upper (K)

TABLE 2

H I PN Line Fluxes[a]

Wavelength[b] (Å)	NGC 1535	NGC 2022	NGC 2392	NGC 3242E	NGC 3242SE	NGC 3242H	NGC 6210E1	NGC 6210E7	NGC 6543	NGC 6572C	NGC 6572E	Identification
11618	0.645	1.43	0.461	4.16	2.16	···	1.19	···	···	···	···	?
11664	0.167	0.218	···	0.646	0.344	···	···	···	···	···	···	He I
11892	···	···	···	···	···	···	···	···	0.668	15.3	17.9	He I
11970	···	···	···	0.153	···	···	0.909	···	1.25	12.3	9.3	?
11986	0.489	0.495	···	···	···	···	···	···	···	···	···	He I
12038	···	···	···	···	···	···	···	···	···	1.33	···	?
12057	0.381	···	0.0621	0.580	0.272	···	···	···	···	···	···	?
12147	0.495	0.407	0.132	1.68	···	···	···	···	···	···	···	?
12529	···	···	···	···	0.255	···	1.01	···	1.13	21.4	14.5	He I
12566	···	0.0616	0.200	···	0.106	···	···	···	0.306	1.09	1.10	[Fe II]
12784	0.258	···	0.329	0.568	1.19	0.231	4.14	0.158	4.80	49.2	32.9	He I
12817	6.33	3.77	6.27	18.9	24.6	3.47	68.9	2.91	70.3	736	529	Pa5 (Pa Beta) H I
12977	···	···	···	···	···	···	···	···	···	5.81	6.46	He I
12994	2.92	···	···	···	···	0.112	···	···	···	14.3	···	He I
13118	0.538	···	···	0.597	0.282	0.113	···	···	···	1.29	1.10	?
13155	···	···	···	···	···	···	···	···	···	2.95	3.24	O I

TABLE 2—*Continued*

Wavelength [b] (Å)	NGC 1535	NGC 2022	NGC 2392	NGC 3242E	NGC 3242SE	NGC 3242H	NGC 6210E1	NGC 6210E7	NGC 6543	NGC 6572C	NGC 6572E	Identification
21310	...	...	...	0.0919	0.122	...	...	...	0.094	1.16	0.302	?
21658	3.24	1.15	2.02	3.88	4.51	1.07	24.0	1.30	17.3	153	115	Br7 (Brγ) H I
21892	...	0.336	0.152	0.793	0.391	...	0.314	...	...	...	...	?
21993	...	...	...	...	...	...	...	...	0.0974	1.74	1.83	U[c]
22858	...	...	...	0.299	0.216	0.116	0.846	...	0.542	4.99	4.36	U[c]
23359	...	...	...	...	...	...	...	...	...	0.502	0.604	Pf ?
23395	...	...	...	...	...	...	...	...	...	0.472	0.444	Pf ?
23443	...	...	...	...	...	...	...	...	0.0958	0.974	0.772	Pf ?
23468	...	...	...	0.244	...	...	...	...	...	...	...	?
23489	...	...	...	...	...	...	0.354	...	...	1.24	1.10	Pf ?
23541	...	...	...	...	...	...	0.220	...	0.0998	1.52	1.37	Pf28 H I
23596	...	...	...	...	...	...	0.360	...	0.240	1.39	1.21	Pf27 H I
23665	...	...	...	...	...	...	0.306	...	0.0232	1.52	1.36	Pf26 H I
23739	...	...	...	...	...	...	0.468	...	0.246	1.99	1.65	Pf25 H I
23828	...	...	...	...	...	...	0.434	...	0.233	1.92	2.05	Pf24 H I
23920	0.438	...	...	...	...	...	0.492	...	0.287	2.43	2.54	Pf23 H I
24031	0.502	...	...	...	...	...	0.258	...	0.287	2.90	2.65	Pf22 H I
24160	0.359	...	...	...	...	...	0.443	...	0.352	3.29	2.91	Pf23 H I

[a]These are the measured wavelengths, with a 1 σ error of $\lesssim$ 5Å.
[b]Fluxes are in units of 10^{-14} erg cm^{-2} s^{-1}, and have not been corrected for extinction.
[c]Unidentified lines observed in several other PNe (see text).

TABLE 3—*Continued*

Wavelength [b] (Å)	NGC 6803E	NGC 6826SW	NGC 6826SWH	NGC 7009N	NGC 7009W	NGC 7662	IC 351	IC 418C	IC 418E	IC 418H	Identification
14562	...	...	...	...	...	0.0793	...	...	...	...	?
14616	...	...	...	...	...	0.0621	...	...	...	...	?
14760	1.08	...	...	1.84	...	0.340	1.14	...	...	...	?
14881	0.611	0.316	...	...	...	...	...	...	...	...	?
14910	...	...	...	...	...	...	...	...	1.09	...	Br? H I
14942	...	...	...	...	...	...	...	...	1.06	...	Br? H I
14960	...	...	...	...	...	...	...	...	0.796	...	Br25 H I
15000	...	...	...	...	...	...	...	1.28	1.20	...	Br24 H I
15033	1.05	0.273	...	...	0.183	...	...	1.18	2.53	...	Br23 H I
15076	1.13	0.236	...	0.549	0.154	0.0572	...	1.80	3.55	...	Br22 H I
15126	0.759	0.135	...	0.425	...	...	...	1.32	2.79	...	Br21 H I
15184	1.04	0.198	...	0.463	0.0942	...	0.260	1.20	3.30	...	Br20 H I
15254	1.08	0.331	...	0.444	0.161	0.0583	0.230	2.10	4.03	...	Br19 H I
15335	1.59	0.313	...	0.510	0.140	0.0505	0.308	2.26	4.78	...	Br18 H I
15432	1.60	0.662	0.452	0.517	0.210	0.0605	0.349	2.12	5.31	...	Br17 H I
15549	2.17	0.410	0.177	0.759	0.208	0.0554	0.402	2.47	6.26	...	Br16 H I
15693	2.38	0.550	0.244	1.14	0.232	0.113	0.407	3.52	7.11	...	Br15 H I
15826	0.609	0.196	...	...	0.262	...	0.410	...	...	...	?
15875	3.20	0.681	0.320	1.25	0.264	0.0968	0.400	4.69	10.0	...	Br14 H I
16020	...	...	...	...	0.156	...	...	...	...	...	?
16102	3.90	0.910	0.413	1.39	0.408	0.104	0.634	5.51	12.8	...	Br13 H I
16401	5.03	1.19	0.507	1.71	0.433	0.131	0.661	7.02	15.3	...	Br12 H I
16432	...	...	...	...	...	...	...	...	...	...	[Fe II]
16690	0.29	0.420	...	...	0.218	...	0.297	...	...	...	?
16801	5.90	1.34	0.657	2.28	0.575	0.175	0.860	8.92	19.6	...	Br11 H I
16920	...	...	...	0.395	...	...	...	...	...	...	?
16997	3.37	1.15	0.247	0.930	0.399	0.0401	0.367	3.26	6.79	...	He I
17111	...	...	...	...	...	...	...	...	...	...	?
17356	8.19	1.68	0.918	3.14	0.808	0.242	1.37	12.7	29.8	...	Br10 H I
17640	0.341	...	...	...	...	...	0.391	...	...	...	?
17733	...	...	...	...	...	...	...	...	...	...	?
19446	18.9	3.08	1.43	2.41	0.481	0.238	0.836	31.7	75.0	0.373	Br8 H I
19549	1.82	0.39	0.159	0.359	0.104	...	...	2.48	5.53	...	He I
20006	0.534	...	...	...	0.0856	...	0.356	...	...	...	?

TABLE 4

H I PN LINE FLUXES[a]

Wavelength [b] (Å)	IC 2149C	IC 2149E	IC 3568	IC 4593C	IC 4593E	J 320C	J 320N1	J 320P15	M 4-18	Identification
11539	...	...	...	...	...	...	...	...	2.27	?
11581	...	...	...	...	...	...	...	...	5.59	?
11618	...	...	0.145	...	...	0.351	...	...	...	?
11664	...	...	...	...	0.184	...	...	...	...	He I
11798	...	...	...	...	...	...	...	...	...	He I
11892	2.38	0.994	...	...	...	...	...	...	3.36	He I
11986	2.92	1.15	0.178	...	...	...	...	...	8.00	He I
12038	1.19	...	...	...	...	...	...	...	...	?
12057	...	0.594	0.215	...	...	...	...	...	...	?
12112	...	...	...	...	...	...	...	...	1.70	?
12194	...	...	...	...	...	...	...	...	0.429	?
12228	...	...	...	...	...	...	...	...	0.595	?
12440	...	...	...	...	...	...	...	...	0.743	?
12529	1.95	1.17	0.187	...	...	...	...	...	1.59	He I
12566	...	...	...	...	...	...	...	...	1.26	[Fe II]
12784	3.62	3.50	0.829	2.41	0.958	0.446	0.518	0.495	2.93	He I
12817	65.9	65.8	13.8	33.0	14.8	7.82	8.23	8.69	30.6	Pa5 (Pa Beta) H I
12977	...	...	0.165	0.935	...	...	...	...	0.622	He I
12994	...	0.936	0.312	...	...	...	...	...	...	He I
13118	...	0.428	0.127	...	...	...	...	...	...	?
13034	...	...	...	...	...	...	...	...	0.525	?
13155	...	...	...	...	...	...	...	...	0.856	O I

TABLE 4—*Continued*

Wavelength [b] (Å)	IC 2149C	IC 2149E	IC 3568	IC 4593C	IC 4593E	J 320C	J 320N1	J 320P15	M 4-18	Identification
20443	...	...	...	...	...	...	...	...	...	He I
20580	11.1	13.2	1.20	4.49	2.16	0.292	0.309	0.330	5.21	He I
20855	...	...	...	...	...	...	...	...	0.446	?
21015	...	...	...	...	...	...	...	...	0.297	?
21089	...	...	...	...	...	...	...	...	0.318	?
21124	1.27	0.732	0.146	0.427	...	...	...	...	0.835	He I
21658	17.3	16.7	3.08	8.74	4.19	1.88	1.88	1.66	7.74	?
21982	...	0.126	...	...	...	...	...	...	...	?
23489	...	...	...	...	...	...	...	...	...	Pf ?
23541	...	0.304	...	...	...	...	...	...	...	Pf28 H I
23596	...	0.205	...	...	...	...	...	...	...	Pf27 H I
23665	...	0.107	...	...	...	...	...	...	...	Pf26 H I
23739	...	0.237	...	...	...	...	...	...	...	Pf25 H I
23828	...	0.338	...	...	...	...	...	...	...	Pf24 H I
23920	...	0.316	...	...	...	...	...	...	...	Pf23 H I
24031	...	0.414	...	...	...	...	...	...	...	Pf22 H I
24160	...	0.255	...	...	...	...	...	...	...	Pf23 H I

[a]These are the measured wavelengths, with a 1 σ error of $\lesssim 5$Å.
[b]Fluxes are in units of 10^{-14} erg cm^{-2} s^{-1}, and have not been corrected for extinction.
[c]Unidentified lines observed in several other PNe (see text).

TABLE 5—*Continued*

Wavelength [b] (Å)	NGC 40	NGC 2440NE	NGC 2440N	NGC 2440T	NGC 6720A	NGC 6720B	NGC 7027T	NGC 7027WT	BD+30° 3639H2	BD+30° 3639N	BD+30° 3639OE	Identification
12618	...	...	...	...	.155	...	...	.314	.397	...	.837	H_2 (3,1) S(0) +(9,6) S(1) +(4,2) S(3)
12696	...	...	...	...	.0276	...	...	...	...	...	...	H_2 (8,5) O(3)
12757	...	...	...	...	.144	...	...	...	...	...	...	?
12784	.697	...	.889	.145	.355	...	40.5	3.71	.656	14.0	.193	He I
12817	18.4	.553	21.5	4.94	4.75	...	946	72.6	29.8	811	9.87	Pa5 (Pa Beta) H I
12869	...	...	...	...	.0665	...	...	.172	...	...	...	H_2 (2,0) Q(7)
12912	...	...	...	...	...	...	3.65	...	...	...	...	?
12928	...	...	...	...	:0305	...	...	...	.0514	.819	.243	H_2 (2,0) O(2)
12977	...	...	...	...	.0610	...	...	...	.0468	1.59	...	He I
12994	...	...	...	.558	...	...	77.6	20.8	...	...	...	?
13108	...	...	...	...	...	...	...	.819	.302	...	.651	H_2 (5,3) S(5) +(4,2) S(1)
13155	...	...	...	...	...	...	...	.875	1.34	7.79	.637	O I + H_2 (9,6) Q(1) ?
13237	...	...	...	...	...	...	...	...	...	...	.196	H_2 (3,1) Q(3)
14760	...	...	...	...	...	...	84.4	5.71	...	...	...	?
14881	...	...	...	...	...	...	15.8	2.04	...	...	...	?
14925	...	...	...	...	...	...	...	...	...	...	.468	H_2 (5,3) Q(1)
14976	...	...	...	...	...	...	...	...	...	...	.240	H_2 (5,3) Q(2)
15010	...	...	...	...	...	...	...	...	...	...	.380	H_2 (6,4) S(1)
15033	...	...	...	...	...	...	11.4	...	.272	4.91	...	Br 23 H I
15051	...	...	...	...	...	...	...	...	...	...	.494	H_2 ?
15076	...	...	...	...	...	...	7.82	.926	.453	6.33	...	Br 22 H I
15091	...	...	...	...	...	...	...	...	...	...	.413	H_2 ?
15126	...	...	...	...	...	...	8.94	.890	...	5.31	...	Br21 H I
15142	...	...	...	...	...	...	...	...	.326	...	...	H_2 (5,3) Q(4)
15184	.272	...	...	...	...	...	11.0	1.21	...	7.12	...	Br20 H I
15205	...	...	...	...	...	...	...	...	.421	...	...	H_2 (3,1) O(5)
15221	...	...	...	...	...	...	...	...	...	...	.348	?
15254	.287	...	.182	...	...	...	11.6	1.01	.362	8.00	...	Br19 H I
15335	.289	...	.222	...	...	...	14.5	1.77	.376	10.3	...	Br18 H I
15334	...	...	...	...	...	...	...	...	...	...	.174	?
15432	.312	...	.192	...	...	...	14.3	1.47	.462	10.5	...	Br17 H I
15549	.460	...	.297	...	...	...	18.5	1.79	.459	10.7	...	Br16 H I

TABLE 5—*Continued*

Wavelength [b] (Å)	NGC 40	NGC 2440NE	NGC 2440N	NGC 2440T	NGC 6720A	NGC 6720B	NGC 7027T	NGC 7027WT	BD+30° 3639H2	BD+30° 3639N	BD+30° 3639OE	Identification
19446	···	.112	3.40	.831	.598	.103	157	9.31	2.23	40.4	1.24	Br8 H I + H_2 (1,0) S(5)
19549	···	···	···	···	···	···	25.5	···	···	···	···	He I
19570	···	.556	.443	.355	2.18	.748	···	8.2	2.95	5.95	5.20	H_2 (1,0) S(3)
19624	···	···	.123	···	···	···	···	···	.121	···	···	H_2 (8,6) O(2)
19703	···	···	···	···	···	···	···	···	.212	···	.228	H_2 (8,6) O(2)
19868	···	···	···	···	···	···	···	···	.0747	···	···	H_2 (9,7) S(0)
20217	···	···	···	···	···	···	···	···	···	···	.165	H_2 (7,5) O(5)
20275	···	···	···	···	···	···	···	···	···	···	.211	H_2 ?
20334	···	.332	.286	.280	1.52	.265	2.66	2.27	1.21	1.81	2.08	H_2 (1,0) S(2)
20373	···	···	.127	···	···	···	6.30	···	···	···	···	?
20411	···	···	···	···	···	···	···	···	.130	···	.410	H_2 (8,6) O(3)
20580	2.92	.0728	1.30	.273	.404	···	70.5	5.51	.958	55.9	.569	He I
20643	···	···	···	···	.0825	···	2.46	···	.141	···	.074	?
20732	···	0.0564	···	···	.226	···	···	.45	.649	···	.915	H_2 (2,1) S(3)
20847	···	···	···	···	···	···	···	···	.0885	···	···	H_2 (9,7) Q(2)
21001	···	···	···	···	···	···	···	···	.077	···	···	H_2 (9,7) Q(3)
21023	···	···	···	···	···	···	···	.207	···	···	···	?
21086	···	···	···	···	···	···	···	···	.208	···	···	?
21124	.146	···	.236	.0511	···	···	15.8	1.34	.146	1.62	···	He I
21218	.431	.821	.918	.644	4.03	.645	12.2	7.25	3.67	5.35	5.57	H_2 (1,0) S(1)
21268	···	···	···	···	···	···	···	···	···	···	.0886	H_2 ?
21340	···	···	···	···	···	···	···	···	.0741	···	···	?
21380	···	···	···	···	···	···	···	···	.0584	···	···	?
21409	···	···	···	···	···	···	···	.223	···	···	···	?
21462	···	···	···	···	···	···	···	.160	.0891	···	···	?
21542	···	···	···	···	.243	···	···	.223	.376	···	.471	H_2 (2,1) S(2)
21658	6.27	.103	4.44	1.02	1.22	···	238	20.3	5.26	164	1.72	Br7 (Brγ) H I
21822	···	···	···	···	···	···	···	···	.126	···	···	?
21892	···	···	.836	.228	···	···	31.6	1.55	.119	···	···	?
21993	.611	···	···	···	.0883	···	7.27	.913	···	1.69	···	U[c]
22014	···	···	.030	···	.127	···	···	···	.447	···	.408	H_2 (3,2) S(3)
22099	···	···	···	···	···	···	···	···	.113	.399	···	H_2 (8,6) O(5)
22114	···	···	···	···	···	.0548	···	···	···	···	.218	?

TABLE 6

H_2 + H I PN Line Fluxes[a]

Wavelength[b] (Å)	Hb 12 core	Hb 12 3.″7E[c]	Hb 12 3.″7E 2″S[c]	IC 2003	I21282 +5050	M 1-16 core	M 1-16 1″S	M 1-92	M 2-9 Core	M 2-9 N Knot[d]	M 2-9 Lobe O[d]	Vy 2-2	Identification
11621	···	0.0668	0.0751	5.55	···	0.559	1.42	0.399	···	···	···	2.78	?
11665	···	0.0480	0.0491	0.925	···	0.138	0.237	0.854	···	···	···	1.92	?
11687	···	0.0300	0.0400	···	···	···	···	···	···	···	···	···	H_2 (8,5) S(0)
11748	···	···	···	···	···	0.0807	···	1.73	···	···	···	···	?
11784	···	···	···	···	···	0.0847	0.142	0.768	···	···	···	···	?
11822	···	···	···	···	···	···	···	1.51	···	···	···	···	?
11854	···	0.0839	0.0311	···	···	0.0882	···	···	···	···	···	···	H_2 (3,1) S(3)
11892	···	0.0440	0.0300	0.568	···	0.148	0.372	1.32	3.29	0.275	···	2.39	He I, [Fe II], Fe I, H_2 (2,0) S(0)
11970	···	···	···	···	···	0.0901	0.188	···	3.29	···	···	11.0	?
11986	23.55	···	···	···	···	···	···	1.03	···	···	···	···	He I
12038	···	···	···	···	···	···	0.136	0.955	···	···	···	···	?
12069	···	0.0801	0.0560	···	···	···	···	···	···	···	···	···	H_2 (3,1) S(2)
12087	···	···	···	···	···	···	···	0.664	···	···	···	0.984	?
12143	···	···	0.00405	0.476	···	0.0484	···	···	···	···	···	···	H_2 (8,5) Q(3)
12213	···	···	0.0221	···	···	···	···	···	···	···	···	···	H_2 (11,7)O(3)
12258	···	0.0658	0.0131	···	···	···	0.236	···	···	···	···	···	H_2 (4,2) S(5)
12294	4.40	···	···	···	···	···	···	···	···	···	···	···	?
12329	···	0.127	0.072	···	···	···	···	···	···	···	···	···	H_2 (3,1) S(1)
12383	···	0.0839	0.0761	···	···	0.0469	···	···	···	4.05	···	···	H_2 (2,0) Q(1)
12420	···	0.0641	···	···	···	···	···	···	···	···	···	···	H_2 (2,0) Q(2)+(4,2) S(4)
12469	···	0.0658	0.0230	···	···	···	···	···	···	···	···	···	H_2 (2,0) Q(3)
12529	50.2	0.0668	0.0221	···	···	0.0644	0.325	···	6.13	···	···	23.7	He I
12566	4.71	0.204	0.467	···	···	···	···	1.65	18.6	3.85	···	10.0	[Fe II]

TABLE 6—*Continued*

Wavelength [b] (Å)	Hb 12 core	Hb 12 3.″7E[c]	Hb 12 3.″7E 2″S[c]	IC 2003	I21282 +5050	M 1-16 core	M 1-16 1″S	M 1-92	M 2-9 Core	M 2-9 N Knot[d]	M 2-9 Lobe O[d]	Vy 2-2	Identification
15432	21.4	···	···	0.397	···	···	0.215	···	2.85	···	···	8.65	Br17 H I
15549	···	···	···	0.562	···	0.102	0.239	···	6.35	···	···	10.9	Br16 H I
15567	···	0.0290	0.0341	···	···	···	···	···	···	···	···	···	?
15610	···	0.130	0.0770	···	···	···	···	···	···	···	···	···	H_2 (7,5) S(3) + (5,3) Q(7)
15693	29.2	···	···	0.757	···	0.176	0.348	···	8.10	···	···	13.6	Br15 H I
15875	36.4	···	···	0.790	···	0.203	0.354	···	13.1	···	···	17.6	Br14 H I
15877	···	0.0781	0.0660	···	···	···	···	···	···	···	···	···	H_2 (7,5) S(2)
15920	···	0.0321	···	···	···	···	···	···	···	···	···	···	?
16003	···	0.0791	0.108	···	···	···	···	0.683	2.63	0.341	···	···	[Fe II]
16102	46.8	0.0641	0.045	0.770	···	0.216	0.402	1.17	10.7	0.143	···	18.9	Br13 H I
16149	···	0.0962	0.072	···	···	···	···	···	···	···	···	···	H_2 (6,4) Q(3)
16204	···	0.0781	···	···	···	···	···	···	···	···	···	···	?
16231	···	···	···	···	···	···	0.177	0.352	···	···	···	···	?
16269	···	0.0471	···	···	···	···	···	···	···	···	···	···	H_2 (6,4) Q(4)
16401	56.2	···	···	1.23	···	0.301	0.503	1.33	15.3	···	···	25.4	Br12 H I
16432	···	0.160	0.581	···	···	···	0.141	2.30	10.1	4.73	···	8.63	[Fe II]
16584	···	···	···	···	···	0.0846	···	···	···	···	···	···	?
16750	···	0.0740	0.152	···	···	···	···	···	···	···	···	···	H_2 (6,4) O(2)
16801	66.3	0.149	0.116	1.21	···	0.504	0.541	1.27	49.3	···	···	32.1	Br11 H I + [Fe II]?
16867	···	0.829	···	···	···	···	···	···	23.0	···	···	···	H_2 (1,0) S(9) + [Fe II]?
16919	···	···	···	···	···	0.101	0.263	···	···	···	···	···	?
16997	35.5	···	···	···	···	···	···	···	8.21	···	···	17.6	He I
17111	···	···	···	···	···	···	···	···	1.75	0.154	···	···	[Fe II]?
17280	···	0.0757	0.0491	···	···	···	···	···	···	···	···	···	?
17317	···	0.0750	0.048	···	···	···	···	···	···	···	···	···	H_2 (6,4) O(3)
17352	···	0.165	0.0851	···	···	···	···	···	···	···	···	···	H_2 (7,5) Q(2)
17356	91.4	···	···	2.14	···	0.674	0.894	1.49	37.2	···	···	44.9	Br10 H I
17415	···	···	···	···	···	···	···	0.485	40.5	···	···	···	[Fe II]?
17435	···	···	···	···	···	···	···	···	···	···	···	2.44	?
17446	5.02	···	···	···	···	···	···	···	···	···	···	···	C I
17459	···	0.0849	0.072	···	···	···	···	···	···	···	···	···	H_2 (1,0) S(7)
19446	···	···	···	2.28	···	0.753	2.27	5.22	77.7	0.935	0.728	84.1	Br8 H I + H_2 (2,1) S(5)
19541	28.9	···	···	···	···	···	···	···	···	0.209	···	17.3	He I
19570	···	0.224	0.187	···	0.913	0.0897	0.330	5.87	23.0	0.132	3.59	···	H_2 (1,0) S(3), [Fe II]?

TABLE 6—*Continued*

Wavelength [b] (Å)	Hb 12 core	Hb 12 3.″7E[c]	Hb 12 3.″7E 2″S[c]	IC 2003	I21282 +5050	M 1-16 core	M 1-16 1″S	M 1-92	M 2-9 Core	M 2-9 N Knot[d]	M 2-9 Lobe O[d]	Vy 2-2	Identification
23400	···	···	···	···	···	···	···	···	···	···	···	1.09	Pf H I
23448	···	0.0501	···	0.328	···	···	···	···	···	···	0.0988	···	H_2 (4,3) S(3) + (9,7) O(4)
23468	···	···	···	···	···	···	0.350	···	···	···	···	···	?
23475	···	···	···	···	···	···	···	···	···	···	···	3.26	Pf H I
23541	3.45	···	···	···	···	···	···	···	···	···	···	2.01	Pf28 H I
23551	···	0.089	···	···	···	···	···	5.06	···	···	0.177	···	CO, H_2 (2,1) S(0)
23596	3.14	···	···	···	···	···	···	···	···	···	···	1.69	Pf27 H I
23665	3.45	···	···	···	···	···	···	···	···	···	···	2.02	Pf26 H I
23739	3.14	···	···	···	···	···	···	···	···	···	···	2.19	Pf25 H I
23828	4.40	···	···	···	···	···	···	···	···	···	···	3.79	Pf24 H I
23861	···	0.133	0.0489	···	···	···	···	···	···	···	0.426	···	H_2 (3,2) S(1)
23920	5.34	···	···	0.145	···	···	···	···	···	···	···	3.80	Pf23 H I
24031	5.65	···	···	0.101	···	···	···	···	···	···	···	4.21	Pf22 H I
24065	···	0.389	0.149	0.243	1.39	0.963	1.03	3.00	···	0.165	5.20	6.36	H_2 (1,0) Q(1)
24130	···	0.154	0.0590	···	0.326	0.391	0.285	2.73	···	0.110	1.77	2.17	H_2 (1,0) Q(2)
24160	···	···	···	···	···	···	···	···	···	···	···	4.10	Pf23 H I
24231	···	0.251	0.136	···	0.841	0.475	0.663	···	···	0.165	3.69	2.96	H_2 (1,0) Q(3)

[a]These are the measured wavelengths, with a 1 σ error of $\lesssim$ 5Å.
[b]Fluxes are in units of 10^{-14} erg cm^{-2} s^{-1}, and have not been corrected for extinction.
[c]See Hora & Latter 1996 for an explanation of slit positions
[d]See Hora & Latter 1994 for an explanation of slit positions
[e]Unidentified lines observed in several other PNe (see text).

TABLE 7—*Continued*

Wavelength [b] (Å)	NGC 2346	AFGL 618 2.4"E	AFGL 618 core	AFGL 2688lobe[c]	AFGL 2688torus[c]	J 900 jet	J 900 lobe	K4-45	M 1-78	Identification
12869	...	0.265	...	...	...	...	...	...	...	H_2 (2,0) Q(7)
12977	...	...	...	...	...	...	...	...	1.01	He I
13155	...	...	0.496	...	...	...	...	...	1.78	O I + H_2 (9,6) Q(1) ?
14881	...	0.212	...	...	...	...	...	...	...	?
15033	...	...	...	...	...	...	...	...	1.45	Br 23 H I
15076	...	...	...	...	...	...	...	...	1.93	Br 22 H I
15126	...	...	...	...	...	...	...	...	1.83	Br21 H I
15190	...	...	...	...	...	...	...	...	2.01	?
15205	...	0.149	...	...	...	...	...	...	...	H_2 (3,1) O(5)
15257	...	...	...	...	...	...	...	...	2.00	?
15280	...	0.122	...	...	...	...	...	...	...	?
15334	...	0.120	0.375	...	...	...	...	...	2.85	?
15432	...	...	...	...	...	...	...	...	3.22	Br17 H I
15549	...	...	...	...	...	...	...	...	4.26	Br16 H I
15877	...	...	0.149	...	...	...	...	...	6.14	H_2 (7,5) S(2) + Br 14 H I
16003	...	...	0.162	...	...	...	...	...	...	?
16102	...	...	...	...	...	...	...	...	7.97	Br 13 H I
16401	...	...	0.440	...	...	...	...	...	10.1	Br 12 H I
16432	...	1.07	1.04	...	...	...	...	...	3.45	[Fe II]
16766	...	0.198	...	...	...	...	...	...	...	?
16798	...	...	0.718	...	...	...	...	...	14.7	Br11 H I
16867	...	0.605	0.808	...	0.420	...	...	...	...	H_2 (1,0) S(9)
17002	...	...	...	...	...	...	...	...	6.68	He I
17131	...	0.465	0.514	...	0.228	...	...	...	...	H_2 (1,0) S(8)
17356	...	...	0.910	...	...	...	...	...	22.2	Br10 H I
17467	0.412	2.41	3.09	1.31	1.80	...	...	...	...	H_2 (1,0) S(7) + (7,5) Q(3)
17866	...	1.38	2.02	0.73	1.20	...	...	...	...	H_2 (1,0) S(6)
19443	0.159	0.489	1.60	0.803	0.720	...	...	...	44.0	Br 8 H I
19541	0.092	...	...	...	...	...	...	...	6.45	He I
19570	0.831	17.1	18.5	8.76	13.2	0.621	0.688	...	...	H_2 (1,0) S(3)
19675	...	0.135	0.171	...	...	...	...	...	...	H_2 ?
20028	...	0.428	...	...	0.228	...	...	...	...	H_2 (2,1) S(4)
20334	0.794	4.67	5.15	2.41	3.84	0.237	0.247	...	1.29	H_2 (1,0) S(2)
20580	...	...	0.325	...	...	0.0316	...	...	75.7	He I

TABLE 8

H_2 EXCITATION ANALYSIS RESULTS

Object/Position	UV Excited	$T_{ex}(J)$[1] (K)	2-1 S(1)/1-0 S(1)	O/P[2]	A_V[3] (mag)
NGC 40	No?[4]	2100±700	....		0
NGC 2346	Yes	1260±200	0.08	2.2±0.5	0
NGC 2440T	Yes?[5]	2020±200	....	2.2±0.4	0
NGC 2440N	Yes	1065±200	0.12	2.6±0.2	0
NGC 2440NE	No?	2010±100	0.09	2.5±0.2	0
NGC 6720A	Yes	1245±100	0.11	2.6±0.4	1±1
NGC 6720B	No?[3]	2000±200	....	3.0±0.5	0
NGC 7026	—[6]	....	....		...
NGC 7027T	Yes	800±200	0.07	2.9±0.7	0
NGC 7027WT	Yes	1325±200	0.08	3.0±0.2	0
AFGL 618C	Yes	1865±300	0.10	3.0±0.5	2±1
AFGL 618E	Yes	2130±300	0.11	3.0±0.5	2±2
AFGL 2688	No	2300±100	0.09	3.0±0.4	5+10/−5
BD+30°3639N	Yes[5]	1255±300	0.18	2.8±0.5	6
BD+30°3639E	Yes	1350±200	0.18	2.7±0.2	2±1
BD+30°3639H2	Yes	1070±100	0.18	2.3±0.2	6±5
Hb 12 2.4E	Yes	1395±450	0.47	1.7±0.2	3.7+1.5/−1.0
Hb 12 2.4E 1.0S	Yes	1395±500	0.47		3.7+1.5/−1.0
IC 2003	—	....	....		...
I21282+5050	No?[4]	700±400	....		4
J 900J	No	2200±100	0.14		0
J 900L	No	2500±100	0.17		0
M 1-16C	Yes	600±100	....	3.0±0.5	3
M 1-16S	Yes	630±100	0.24	3.0±0.5	0
M1-92	No?[4]	450+650/−450	....		0
M 2-9N	—	....	0.20		5
M 2-9L	Yes	1220±50	0.11	2.8±0.2	5+7/−5
Vy 2-2	Yes	730±200	0.24		1

[1]For UV excited spectra $T_{ex}(J)$ is the rotational excitation temperature. For collisionally excited spectra $T_{ex}(J) = T_{ex}(v)$.

[2]Listed only for those objects with enough lines well detected to make an estimate of the O/P ratio.

[3]Value of visual attenuation used to deredden the H_2 spectra for the excitation analysis (as determined from the H_2 lines only and using a standard interstellar extinction law; Rieke & Lebofsky 1985). Entries with errors shown are determined to greater accuarcy than those without, which should be considered highly uncertain. In no case does the value of A_V change the basic results of the analysis.

[4]v = 1 detections only.

[5]v = 8 transition(s) detected.

[6]— means there are not enough lines detected to make an excitation analysis.